Journal of Neurochemistry

JNC

JOURNAL OF NEUROCHEMISTRY | 2018 | 147 | 626–646

doi: 10.1111/jnc.14614

ORIGINAL ARTICLE

Distribution and development of molecularly distinct perineuronal nets in visual thalamus

Ubadah Sabbagh*†[1], Aboozar Monavarfeshani*‡[1], Kaiwen Su*, Masoud Zabet-Moghadam§, James Cole*¶, Eric Carnival*, Jianmin Su*, Mehdi Mirzaei**††‡‡, Vivek Gupta‡‡, Ghasem Hosseini Salekdeh**§§ and Michael A. Fox*‡¶¶

*Developmental and Translational Neurobiology Center, Virginia Tech Carilion Research Institute, Roanoke, Virginia, USA

†Graduate Program in Translational Biology, Medicine, and Health, Virginia Tech, Blacksburg, Virginia, USA

‡Department of Biological Sciences, Virginia Tech, Blacksburg, Virginia, USA

§Center for Biotechnology and Genomics, Texas Tech University, Lubbock, Virginia, USA

¶Translational Neurobiology Summer Undergraduate Research Fellowship, Virginia Tech Carilion Research Institute, Roanoke, Virginia, USA

**Department of Molecular Sciences, Macquarie University, North Ryde, New South Wales, Australia

††Australian Proteome Analysis Facility, Macquarie University, Sydney, New South Wales, Australia

‡‡Department of Clinical Medicine, Macquarie University, Sydney, New South Wales, Australia

§§Department of Systems Biology, Agricultural Biotechnology Research Institute of Iran, Agricultural Research, Education, and Extension Organization, Karaj, Iran

¶¶Department of Pediatrics, Virginia Tech Carilion School of Medicine, Roanoke, Virginia, USA

Abstract

Visual information is detected by the retina and transmitted into the brain by retinal ganglion cells. In rodents, the visual thalamus is a major recipient of retinal ganglion cells axons and is divided into three functionally distinct nuclei: the dorsal lateral geniculate nucleus (dLGN), ventral LGN (vLGN), and intergeniculate leaflet. Despite being densely innervated by retinal input, each nucleus in rodent visual thalamus possesses diverse molecular profiles which underpin their unique circuitry and cytoarchitecture. Here, we combined large-scale unbiased proteomic and transcriptomic analyses to elucidate the molecular expression profiles of the developing mouse dLGN and vLGN. We identified several extracellular matrix proteins as differentially expressed in these regions, particularly constituent molecules of perineuronal nets (PNNs). Remarkably, we discovered at least two types of molecularly distinct Aggrecan-rich PNN populations in vLGN, exhibiting non-overlapping spatial, temporal, and cell-type specific expression patterns. The mechanisms responsible for the formation of these two populations of PNNs also differ as the formation of Cat315$^+$ PNNs (but not WFA$^+$ PNNs) required input from the retina. This study is first to suggest that cell type- and molecularly specific supramolecular assemblies of extracellular matrix may play important roles in the circuitry associated with the subcortical visual system and in the processing of visual information.

Keywords: aggrecan, LGN, perineuronal net, retinogeniculate, thalamus, visual.

J. Neurochem. (2018) **147**, 626–646.

Cover Image for this issue: doi: 10.1111/jnc.14203.

Received May 18, 2018; revised manuscript received August 10, 2018; accepted October 9, 2018.

Address correspondence and reprint requests to Michael A. Fox, Developmental and Translational Neurobiology Center, Virginia Tech Carilion Research Institute, Roanoke, VA, USA. E-mail: mafox1@vtc.vt.edu (or) Ghasem Hosseini Salekdeh, Molecular Systems Biology, Royan Institute for Stem Cell Biology and Technology, Tehran, Iran. E-mail: h_salekdeh@abrii.ac.ir

[1]These authors contributed equally to this work.

Abbreviations used: dLGN, dorsal lateral geniculate nucleus; ECM, extracellular matrix; IGL, intergeniculate leaflet; IHC, immunohistochemistry; ISH, *in situ* hybridization; LGN, lateral geniculate nucleus; PNN, perineuronal net; RGC, retinogeniculate; RRID, research resource identifier; vLGN, ventral lateral geniculate nucleus.

ORIGINAL ARTICLE

Visual information is transmitted to over forty subcortical regions of the mammalian brain by retinal ganglion cells (RGCs) (Morin and Studholme 2014; Martersteck *et al.* 2017; Monavarfeshani *et al.* 2017b). One such region is the visual thalamus, which consists of three distinct nuclei: the dorsal lateral geniculate nucleus (dLGN), the ventral LGN (vLGN), and the intergeniculate leaflet. While all three nuclei are densely innervated by RGC axons, each is innervated by unique populations of RGC subtypes, of which more than thirty have been identified in rodents (Sanes and Masland 2015; Baden *et al.* 2016; Rheaume *et al.* 2018). Not only do different subtypes of RGCs project to each nucleus, but the anatomical and physiological properties of nerve terminals formed by these RGCs differ significantly in each region (Hammer *et al.* 2014): retinal terminals in vLGN are small and functionally weak, whereas those in dLGN are large and elicit strong excitatory post-synaptic potentials in thalamocortical relay cells (Hammer *et al.* 2014). Additionally, retinal axons form at least two distinct types of retinogeniculate synapses in dLGN, a characteristic of these axons not found in other retinorecipient nuclei: simple, in which a single large retinal axon synapses onto a relay cell dendrite, and complex, in which many retinal axons converge onto a single dendritic site (Hammer *et al.* 2015; Morgan *et al.* 2016). Moreover, differences in synaptic connectivity between these visual thalamic nuclei are not limited to retinal inputs, as each region is innervated by diverse cohorts of non-retinal axons (Monavarfeshani *et al.* 2017b).

The striking differences in connectivity and synaptic architecture in visual thalamic nuclei suggest the existence of target-specific mechanisms that regulate the unique development of synapses and circuits in each region (Monavarfeshani *et al.* 2018). Outside of visual thalamus, a diverse number of transmembrane adhesion molecules, growth factors, and extracellular matrix (ECM) proteins regulate the targeting, differentiation, refinement, and maturation of nerve terminals (Waites *et al.* 2005; Fox and Umemori 2006; Sanes and Yamagata 2009; Yogev and Shen 2014). Much less is known about molecular signals responsible for the targeting of retinal axons to visual thalamus (Osterhout *et al.* 2011; Su *et al.* 2011), and the molecular mechanisms driving synaptogenesis in these regions (Bjartmar *et al.* 2006; Stevens *et al.* 2007; Singh *et al.* 2012; Monavarfeshani *et al.* 2018). To identify synaptogenic cues that may be differentially expressed in vLGN and dLGN, we employed proteomic and transcriptomic analyses of vLGN and dLGN at eye-opening – a time-point corresponding to the emergence of nucleus-specific synaptic profiles in visual thalamus (Hammer *et al.* 2014; Monavarfeshani *et al.* 2018).

To our surprise, one set of cues that we identified as being differentially expressed in these regions of visual thalamus were ECM proteins. ECMs are supramolecular structures made up of densely packed proteins and polysaccharides which contribute essential roles in neuronal migration, neural circuit formation, and synaptic plasticity (Dityatev *et al.* 2010; Dityatev and Rusakov 2011; Frischknecht *et al.* 2012; Risher and Eroglu 2012; Heikkinen *et al.* 2014; Smith *et al.* 2015). A prominent ECM assembly in the mammalian brain is the perineuronal net (PNN), a lattice-like structure ensheathing the soma and proximal dendrites of subsets of neurons (Hockfield *et al.* 1990; Brückner *et al.* 1993; Celio and Blumcke 1994; Celio *et al.* 1998; Yamaguchi 2000). The molecular composition of PNNs varies throughout the brain. However, key constituents of PNNs include chondroitin sulfate proteoglycans (CSPGs), tenascins, hyaluronan, hyaluronan synthases, and hyaluronan and proteoglycan link proteins (HAPLNs) (Zimmermann and Dours-Zimmermann 2008; Kwok *et al.* 2010; Frischknecht *et al.* 2012; Morawski *et al.* 2012; Sorg *et al.* 2016). In many regions of the brain, PNNs primarily ensheath parvalbumin-expressing ($PARV^+$) GABAergic neurons (Härtig *et al.* 1992; Wen *et al.* 2018), influencing the function of these inhibitory interneurons and therefore playing a critical role in regulating plasticity (Frischknecht *et al.* 2009; van't Spijker and Kwok 2017). There have been conflicting data concerning PNNs in the mammalian visual thalamus; studies in cat identified the presence of Aggrecan-rich PNNs whereas human LGN appears to lack of well-defined PNNs and, instead, contains Aggrecan-rich perisynaptic axonal coats (Sur *et al.* 1988; Hockfield *et al.* 1990; Kind *et al.* 1995; Lendvai *et al.* 2012).

Here, our proteomic and transcriptomic profiling data led us away from studying circuit formation and toward exploring the development, distribution, and composition of PNNs in visual thalamus. We discovered that PNNs exist in mouse vLGN but not dLGN. Moreover, two molecularly-distinct populations of PNNs exist within mouse vLGN, each exhibiting distinct regional and cell-specific expression patterns. Lastly, we demonstrate that one population of vLGN PNNs requires the presence of retinal projections for their timely formation, suggesting an activity-dependent mechanism regulating their assembly. Taken together, this study provides a first glimpse into the unique extracellular environment in visual thalamic regions, and raises questions about the roles that ECM molecules and, more specifically PNNs, play in visual circuitry and information processing.

Materials and methods

Animals

Wild type C57BL/6 mice were obtained from Charles River (Wilminutesgton, MA, USA) or Harlan (Indianapolis, IN, USA). We obtained the following mice from Jackson Laboratory (JAX): *Parv-Cre* (JAX #: 008069, RRID:IMSR_JAX:008069), *Thy1-Stop-Yfp* (JAX #: 005630, RRID:IMSR_JAX:005630), *Calb2-Cre* (JAX #: 10774, RRID:IMSR_JAX:010774), *Rosa-Stop-Tdt* (JAX #: 007905, RRID:IMSR_JAX:007905) and *Gad67-GFP* (JAX #: 007673, RRID: IMSR_JAX:007673). $Math5^{-/-}$ (also known as $Atoh7^{-/-}$ [Wang *et al.* 2001]Stock #: 042298-UCD, RRID:MMRRC_042298-UCD), Sst-Ires-Cre (JAX #: 028864, RRID:IMSR_JAX:028864) and

Aldh1l1-EGFP (stock # 011015-UCD, RRID:MMRRC_011015-UCD) mice were obtained from S. Wang, W. Guido (University of Louisville) and S. Robel (Virginia Tech), respectively. Animals were housed in a temperature –controlled environment, in a 12 h dark/light cycle, and with access to food and water *ad libitum*. Both males and females were used in these experiments. All animals and experiments were maintained and performed in compliance with National Institutes of Health guidelines and protocols and were approved by the Virginia Polytechnic Institute and State University Institutional Animal Care and Use Committee (IACUC). This study was not blinded and no randomization was performed. No sample calculation was performed. Except where otherwise stated, n=animals and a minimum of three animals per age were compared in all experiments described in this study.

Protein sample preparation

To extract proteins for proteomic analysis, mice were deeply anesthetized by intraperitoneal injection of tribromoethanol (Avertin, 250 mg/kg) and decapitated. dLGN and vLGN tissues were pooled from P12 mice. Dissected tissues were homogenized and lysed in lysis buffer containing 10 mM Tris-HCl, (pH 7.4), 0.15 M NaCl, 1 mM EDTA, 1% sodium dodecyl sulfate (SDS) in phosphate-buffered saline (PBS). Proteins were extracted and delipidated as described previously (Shevchenko *et al.* 2012). Ice-cold acetone/methanol/tri-n butylphosphate (TBP; 12 : 1 : 1) was added to the samples and centrifuged to precipitate proteins. Pelleted proteins were washed with acetone, methanol, and TBP before being air dried. The Micro BCA™ Protein Assay Kit (Pierce, Rockford, IL, USA; #: 23235) was used per the manufacturer's protocol to determine total protein content.

In-gel digestion

Equal amounts (150 μg) of samples were loaded into lanes of a 4%–12% Bis-Tris gel (Bio-Rad Laboratories, Hercules, CA, USA) and were electrophoresed in Tris-Glycine SDS buffer at 150 V constant for 60 min. Gels were stained with colloidal Coomassie Blue, washed in water, and lanes were cut into 11 equal slices and transferred into a 1.5 mL microfuge tube. In-gel digestion on each slice was carried out as described previously (Shevchenko *et al.* 2006). Briefly, gel slices were washed in milli Q water for 5 min and washed twice in acetonitrile (ACN)/100 mM NH_4HCO_3 (50/50) to destain the gels. Proteins were reduced in 10 mM dithiothreitol at 56°C at 600 rpm for 1 h. Slices were washed in water, alkylated with 50 μL of iodoacetamide solution (55 mM in 40 mM NH_4HCO_3), and incubated in the dark for 30 min. Gel slices were washed in water, 50% CAN, and then 100% ACN before being air-dried. Samples were digested in sequencing grade trypsin (Promega; 12.5 ng/μL in 25 mM NH_4HCO_3) and incubated overnight at 37°C. Peptide extraction was performed twice using 50% ACN containing 0.1% formic acid solution. The extracted peptide solutions were pooled and dried using a speed vacuum centrifuge and the peptides resuspended 0.1% formic acid for further LC-MS/MS analysis.

Nano LC-MS/MS

Peptides extracted from in-gel digestion were analyzed by nano-flow liquid chromatography tandem mass spectrometry (nano-LC-MS/MS) using a LTQ-Velos Orbitrap (Thermo Fisher Scientific, Waltham, MA, USA) mass spectrometer. Chromatographic separation of the peptides was carried out using a Dionex nano-HPLC (Ultimate 3000) with a trapping column (C18, 3 μm, 100 Å, 75 μm × 2 cm) followed by a reverse phase column (C18, 2 μm, 100 Å, 75 μm × 15 cm, nanoViper). Peptides were injected into the trapping column, which was equilibrated with 1% ACN, 0.1% formic acid in MS grade water. Peptides were trapped for 10 min using the loading pump at a flow rate of 3 μL/min, were loaded on to the reverse-phase analytical column, and were eluted using solvents A (2% ACN, 0.1% formic acid in water) and B (98% ACN, 2% water, 0.1% formic acid) at 300 nL/min. A constant gradient was maintained for the first 10 min at 4% solvent B followed by a gradual increase up to 30% solvent B in 20 min. Solvent B was further increased to 60% in 40 min followed by a rapid increase up to 90% over 5 min. The eluted peptides were directed into the nanospray ionization source of the LTQ-Velos Orbitrap with a capillary voltage of ~1.5 kV. Collected spectra were scanned over the *m/z* range of 400–2000 using Fourier transform mass spectrometer (FTMS) with resolution of 15000. A second scan was data dependent on the ion trap mass spectrometer (ITMS) with defined settings to choose the ten most intense ions with dynamic exclusion list size of 200, repeat duration of 30 s, repeat count of 2, and explosion duration of 90 s. To generate MS/MS spectra in the second scan, collision-induced dissociation of the peptide ions at normalized collision energy of 35% was utilized.

Protein identification and quantitative data analysis

RAW files of LC–MS/MS runs were converted to mzXML format using the ReAdW program (http://tools.proteomecenter.org/wiki/index.php?title=Software:ReAdW). mzXML spectra files were searched using GPM software (Global Proteome Machine, version 2.1.1; http://www.thegpm.org)(Craig and Beavis 2004) against UniProtKB/Swiss-Prot mouse protein database. Each mzXML spectra file was also searched against a reversed-sequence database to calculate the false discovery rate (FDR) as protein FDR = (# reverse proteins identified)/(total protein identifications) × 100 (Rabilloud 2003). Additionally, the peptide FDR was calculated as peptide $\text{FDR} = 2 \times \frac{\#\text{reverse peptide identifications}}{\text{total peptide identifications}}$ (Krijgsveld *et al.* 2006). The 11 output files for each replicate were combined to create a single merged result file, and only proteins with FDR < 1% were used for the analysis. The following parameters were used for the search: enzyme: trypsin; allowed missed cleavage: 2; variable modification: methionine oxidation; fixed modification: carbamidomethylation of cysteine; MS and MS/MS mass tolerance: ± 20 ppm and ±0.2 Da, respectively.

For quantitative analysis, normalized spectral abundance factors were used to assess protein abundance (Neilson *et al.* 2013). For each identified protein, k, in sample i, the number of spectral counts was divided by the length of the identified protein. $NSAF_i$ values for each sample i were obtained by normalizing $SpC_k/length_k$ values to the total by dividing by the sum ($SpC_k/length_k$) over all proteins. NSAF mean values for all replicates were applied to calculate protein abundance. A spectral fraction of 0.5 was added to the entire spectral counts for each protein to compensate for null values and allow for log transformation of the NSAF data prior to statistical analysis (McDonald 2009).

Western blot

After intraperitoneal injection of tribromoethanol (Avertin, 250 mg/kg), mice were decapitated and dLGN and vLGN regions were

rapidly dissected in ice-cold PBS. Each biological sample, composed of pooled tissues at least 5 littermates per group littermates per group, was lysed in modified loading buffer containing 50 mM Tris–HCl (pH 6.8), 2% SDS, 10% glycerol. Samples were homogenized, boiled for 10 min, and their insoluble material was removed. The Micro BCA™ Protein Assay Kit (Pierce #: 23235) was used per the manufacturer's protocol to determine protein concentrations. Equal amounts of protein (30 μg) were loaded and separated by 8% sodium dodecyl sulfate–polyacrylamide gel electrophoresis and transferred to a polyvinylidene difluoride membrane as described previously (Fox *et al.* 2007). After blocking polyvinylidene difluoride membranes using 5% non-fat milk in PBS (0.05% Tween), membranes were incubated overnight with primary antibodies (VGLUT1 [Neuromab 75-066, RRID:AB_2187693] 1:400, VGLUT2 [Neuromab 75-067, RRID:AB_2239153] 1:400, GAD67 [EMD Millipore MAB5406, RRID:AB_2278725] 1 : 5000, GAD67/65 [Chemicon AB1511, RRID:AB_90715] 1 : 5000, CALB1 [Swant, Marly, Switzerland CB-38a] 1 : 10 000, CALB2 [Chemicon AB5054] 1 : 5000, ALCAM [R&D System AF1172] 1 : 1000, SEZ6l [R&D System AF4804] 1 : 1000, ACAN [Millipore AB1031] 1 : 500, ACTIN [EMD Millipore MAB1501, RRID: AB_2223041] 1 : 5000), followed by Horseradish peroxidase conjugated secondary antibodies (Jackson ImmunoResearch Laboratories, West Grove, PA, USA). Immunoblotted proteins were detected with enhanced chemiluminescence (ECL) Prime Western Blotting Detection Reagent (Amersham #: RPN2236).

Immunohistochemistry (IHC)

Mice were anesthetized using 12.5 μg/mL tribromoethanol (Avertin) and transcardially perfused with PBS and 4% paraformaldehyde (PFA; pH 7.4). Extracted brains were kept in 4% PFA for 16 h at 4°C, and then incubated for at least 48 h in 30% sucrose. Fixed tissues were then embedded in Tissue Freezing Medium (Electron Microscopy Sciences, Hatfield, PA, USA), and cryosectioned at 16 μm sections on a Leica CM1850 cryostat. Sections were air-dried onto Superfrost Plus slides (Fisher Scientific, Pittsburgh, PA, USA). Sections (n = 3 mice) were allowed to air-dry for 15 min before being incubated in blocking buffer (2.5% bovine serum albumin, 5% Normal Goat Serum, 0.1% Triton-X in PBS) for 1 h. Primary antibodies were diluted in blocking buffer at the following dilutions and incubated on tissue sections at 4°C for 16 h: GAD67 (Millipore MAB5406, RRID:AB_2278725) 1 : 700; IBA1 (Wako 019-19741, RRID:AB_839504) 1 : 1000; VGLUT2 (Synaptic Systems 135402, RRID:AB_2187539) 1 : 500; VGLUT1 (Synaptic Systems 135511, RRID:AB_887879) 1 : 700; GAD67/65 (Chemicon AB1511, RRID:AB_90715) 1 : 500; CALB1 (Swant, CB-38a) 1 : 1000; CALB2 (Chemicon AB5054, RRID:AB_2068506) 1 : 2000; ACAN (Millipore AB1031, RRID: AB_90460) 1 : 200; Cat315 (Chemicon MAB1581, RRID: AB_11214066) 1 : 2000; biotinylated-WFA (Vector Lab B-1355, RRID:AB_2336874) 1 : 1000; Neuropeptide Y (ImmunoStar 22940, RRID:AB_10720817) 1 : 500; NeuN (Chemicon MAB377, RRID: AB_2298772) 1:200, Somatostatin (Chemicon AB5494, RRID: AB_2255374) 1 : 250. Sections were then washed three times PBS and incubated in anti-mouse or anti-rabbit fluorescently conjugated secondary antibodies (Invitrogen Life Technologies, RRID: SCR_008410) diluted in blocking buffer (1 : 1000) for 1 h at 22°C. Tissue sections were then washed at least 3 times with PBS, stained with DAPI (1 : 5000 in water), and mounted using Vectashield (Vector Laboratories, Burlingame, CA, USA). Stains were visualized on a Zeiss LSM 700 confocal microscope. A minimum of three animals for each group were prepared in all IHC experiments.

In situ hybridization (ISH)

Sez6l (clone ID 30362651), *Syt1* (clone ID 5363062) cDNAs were obtained GE Dharmacon. *Gad1* cDNA (nucleotides 1099–2081) was generated using Superscript II Reverse Transcriptase First Strand cDNA Synthesis kit (# 18064014, Invitrogen, La Jolla, CA, USA) according to the manufacturer manual, amplified by PCR using following primers: *F: TGTGCCCAAACTGGTCCT; R: TGGCCGATGATTCTGGTT* (Integrated DNA Technologies), gel purified, and then cloned into a pGEM-T Easy Vector using pGEM-T Easy Vector kit, (cat # A1360, Promega, Madison, WI, USA) according to the kit manual. Riboprobes against *Gad1*, *Syt1* and *Sez6l* mRNAs were generated as described previously (Monavarfeshani *et al.* 2017a). ISH was performed on 16 μm PFA-perfused coronally cryosectioned brain tissue (n = 3 mice) prepared as described above. Tissues were prepared and hybridized at 60°C as previously described (Su *et al.* 2010; Monavarfeshani *et al.* 2018). Bound riboprobes were detected by either horseradish peroxidase (POD)-conjugated anti-DIG or anti-fluorescent antibodies (Roche #: 11426346910 and 11207733910), followed by Tyramide Signal Amplification systems (PerkinElmer #: NEL75300 1KT). Slides were visualized on a Zeiss LSM 700 confocal microscope. Images were acquired with identical parameters were used to compare sections from different genotypes.

Quantitative real time PCR (qPCR)

RNA was extracted and purified using the Aurum™ Total RNA Fatty and Fibrous Tissue kit (Bio-Rad #: 7326870) according to the manufacturer's protocol. Each biological sample represented pooled tissues from 5 to 7 animals of the same group. Purified RNA was used to generate cDNA using the Superscript II Reverse Transcriptase First Strand cDNA Synthesis kit (Invitrogen), which was then used as a template. For quantifying relative mRNA expression levels, qPCR was performed on a CFX Connect Real Time System (Bio-Rad) using the iTaq SYBRGreen Supermix (Bio-Rad #: 1725124) according to the manufacturer's protocol. The following cycling conditions were used with 12.5 ng of cDNA: 95°C for 30 s, 42 cycles of amplification at 95°C for 10 s and 60°C for 30 s, and a melting curve analysis. Relative mRNA quantities were determined using the ΔΔ-CT method (Schmittgen and Livak 2008). A minimum of three biological replicates, each ran in triplicate, were processed for each gene of interest. Primers were: *Alcam F: TCTGCGA TAAGTATTCCAGAGCAC, R: CAGCCAGTAGACGACACCAG; Calb1 F: TTCATTTCGACGCTGACGGA, R:TCCGGTGATAGCTC CAATCC; Calb2 F: GCTTAAGATCTCCGGAGCGG, R: TGTA CCCATTTCCGTCAGCA; Gad1 F: GCTGACATCGACTGCCA ATA, R: CCATCCAACGATCTCTCTCA; Gad2 F: CAGCCTTAGG GATTGGAACA, R: TCCTTCCTGTTTGACTTCAAGG; Myh11 F: CACGGGGGAGCTGGAAAAG, R: AACTTGCCAAAGCGAGAG GA; Pcdh1 F: GCTCACTGACCGAGAAGGTG, R: AGGAGAA CTTCTGGGTTGTCCA; Sez6l F: ATCTGCCCTCCTGTACGACT, R: TCAAAGGCCTCAAAGCGGAT; Slc8a1 F: GGCACGCTA GCTTTCTCTGTC, R: TGACATTCCGAAGATGGCTCC; Syt1 F: CTCCAGACTACCCCAGCAGA, R: GACAAGGGTCGCAACAGTG;*

Vglut1 F: GTGCAATGACCAAGCACAAG, R:CGAAGCAAAGACC CCATAGA; Vglut2 F: ATCATCACCCAGATTCCAGG, R: TGGGAT CAGCATATTGAGGG

RNA sequencing

RNA from dLGN and vLGN was extracted and purified from mice at four different ages (P3, P8, P12, and P25), and processed at the Genomics Research Laboratory at Virginia Tech's Biocomplexity Institute for RNAseq analysis. The RNA sequencing experiment was previously published and the protocol is described in detail in (Monavarfeshani *et al.* 2018).

Intraocular CTB injections

Mice were anesthetized with isoflurane, and 1–2 μL of fluorophore-conjugated cholera toxin beta subunit (CTB, Thermo Fisher Scientific C22841)(1 mg/mL) was injected intravitreally (Su *et al.* 2011). After 2 days, mice were perfused and fixed with 4% PFA, brains were dissected and sectioned (16 μm) a Leica CM1850 cryostat. Sections were stained as described in IHC section above and finally mounted with Vectashield (Vector Laboratories, Burlingame, CA, USA). Images were acquired on a Zeiss LSM 700 confocal microscope.

Statistical analysis

Unless otherwise stated, results are presented as the mean ± SEM. All statistical analyses were performed using GraphPad Prism 7 (RRID:SCR_002798). Comparisons of expression between different groups in Fig. 5 was determined by performing a two-way analysis of variance (ANOVA test) followed by a Bonferroni *post hoc* test. All other statistical analyses presented were performed by Student's *t*-test. No outlier tests or assessments of normality were conducted.

Results

Proteomic and transcriptomic analyses of vLGN and dLGN at eye-opening

To investigate proteomic differences in vLGN and dLGN at eye-opening, we micro-dissected each region from wildtype C57BL/6 mouse brains and extracted protein using a protocol that enriches for extracellular and membrane-associated proteins. Protein samples underwent in-gel digestion and extracted peptides were analyzed by nano-flow liquid chromatography tandem mass spectrometry (nano-LC-MS/MS; Fig. 1a). We identified 1710 proteins that were present in all replicates of vLGN or dLGN samples. To discriminate between the two regions with high confidence, we compared normalized spectral abundance factor (NSAF) values of proteins in either nucleus, and considered p-values ≤ 0.05 as the criterion for significant enrichment (Fig. 1b). We identified 63 proteins enriched in vLGN and 92 enriched in dLGN. We processed all identified proteins by gene ontology (GO) analysis and found that over 50% of peptides detected were membrane– or ECM–associated proteins by GO analysis (Fig. 1c).

We next sought to examine the biological correlation and complementarity between these proteomic profiles and a transcriptomic analyses previously performed on vLGN and dLGN at eye-opening (Monavarfeshani *et al.* 2018). This integrative approach provides more reasonable insight into tissue- and cell-specific functions for a number of reasons. Firstly, the steady-state expression level of a given gene's mRNA and protein is dependent on a balance between rates of synthesis and degradation, both of which are governed by independent mechanisms. Secondly, mRNA levels do not necessarily correlate with protein abundance (Maier *et al.* 2009). Thirdly, mRNA and protein levels may differ because neurons, and the brain regions they reside in, have far-reaching afferents and efferents. For all these reasons, we mapped a total of 1628 proteins obtained from our proteomics analysis to our previously published RNAseq dataset (Monavarfeshani *et al.* 2018) (Fig. 2a). A limitation of this comparison is that the breadth of the proteome accessed by MS was more narrow than that of vLGN and dLGN transcriptomes.

When comparing proteomic and transcriptomic datasets, we observed several trends (which we validated with quantitative real-time PCR [qPCR; Fig. 2b], immunohistochemistry [IHC; Fig. 2c], *in situ* hybridization [ISH; Fig. 2d–f], and Western Blotting [WB; Fig. 2g]). We observed cases where enrichment of a given mRNA and its associated protein product were well-correlated (in a single region of visual thalamus). This concordance was observed with several genes and proteins, including GAD65 and SEZ6L, whose mRNA are both enriched in one thalamic region (Fig. 2d–f), and whose proteins are enriched in the same regions (Fig. 2b–g). However, when mRNA and protein levels appear correlated they are not always generated by the same cell(s). For example, mRNA and protein levels of Vesicular Glutamate Transporter 2 (VGLUT2) were both enriched in dLGN (Fig. 2b and c), however that enrichment likely originates from different sources. While dLGN relay cells generate *Vglut2* mRNA, the translated proteins are transported to their axonal terminals in layer IV of cerebral cortex. Therefore, the bulk of VGLUT2 protein within dLGN is likely not produced by relay cells. Instead, it arises from RGC axon terminals (Land *et al.* 2004; Hammer *et al.* 2014). Thus, the mere fact that the patterns of a given mRNA and protein match in our proteomic and transcriptomic analyses does not necessarily imply generation by the same cell.

Another common pattern that emerged was discrepant expression, meaning a given mRNA or protein was either enriched in one dataset, but not in the other, or that an mRNA and related protein are enriched in opposite regions. For example, glutamate decarboxylase 1 (*Gad1*) mRNA was enriched in vLGN, but its protein (GAD67) was enriched in dLGN. This was not shocking since the dLGN is densely innervated by inhibitory projection neurons residing in the thalamic reticular nucleus (TRN), but contains significantly fewer local GABAergic interneurons than vLGN (Monavarfeshani *et al.* 2017b).

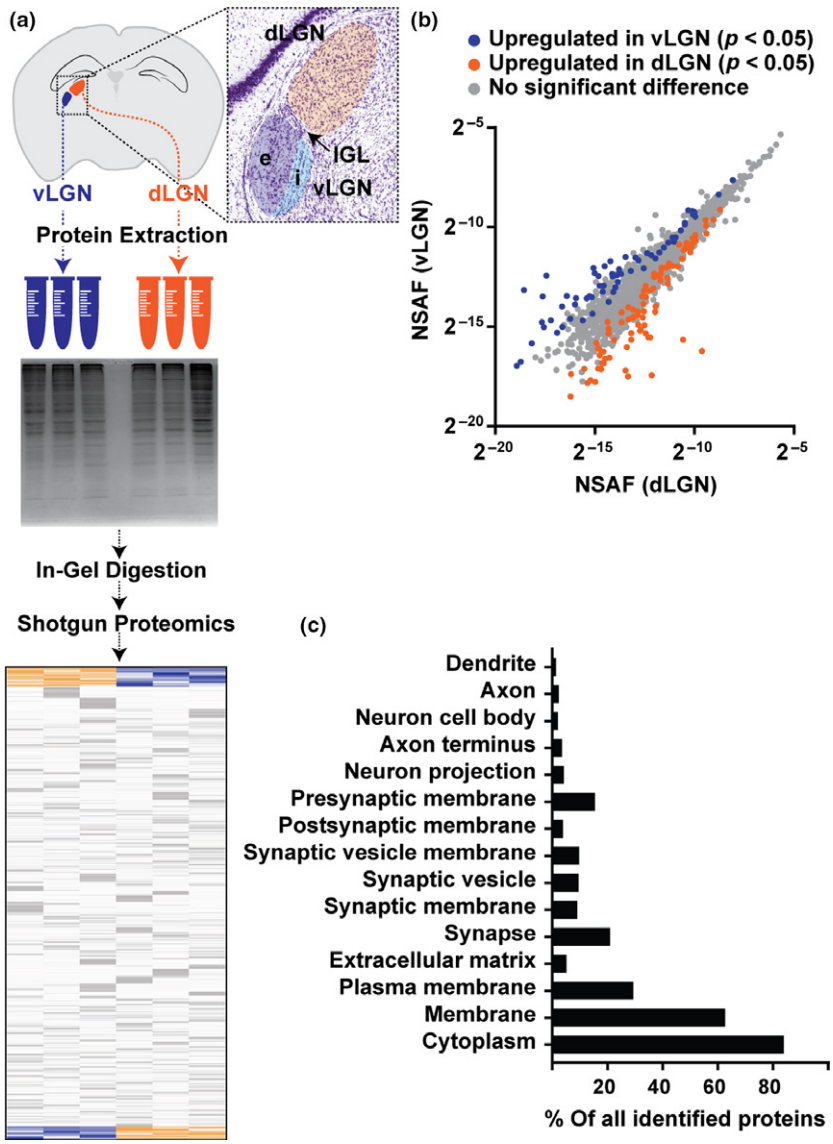

Fig. 1 Differentially expressed proteins in ventral and dorsal lateral geniculate nuclei. (a) Schematic representation of mouse visual thalamus and the protocol used for proteome data acquisition. Inset shows a coronal view of a Nissl-stained mouse brain, adapted from the Allen Brain Atlas (http://www.brain-map.org), with dLGN, intergeniculate leaflet (IGL, vLGNe, and vLGNi highlighted. Heat map illustrates hierarchical clustering of the log-transformed ratios of identified proteins in vLGN and dLGN (blue and orange rows represent differentially expressed proteins). (b) Volcano scatter plot demonstrating differentially expressed proteins significantly upregulated in vLGN (blue) and dLGN (orange). (c) Results of GO analysis for all identified proteins. dLGN – dorsal lateral geniculate nucleus; IGL – intergeniculate leaflet; vLGN – ventral lateral geniculate nucleus; e – external division; i – internal division; NSAF – normalized spectral abundance factor. $n = 3$ mice.

The last pattern to emerge was one in which proteomic analysis failed to capture proteins that should have been abundantly enriched in one region. For example, Vesicular Glutamate Transporter 1 (VGLUT1), a protein present within the abundant corticothalamic nerve terminals in dLGN, was absent from this dataset (Fig. 2g). One possible reason for this is that VGLUT1 proteins could have been lost during the extraction, however that falls short of explaining why similar vesicular associated proteins (i.e. VGLUT2) were successfully captured using the same protocol.

Taken together, these data highlight the importance of cautiously interpreting large-scale proteomic and transcriptomic results when studying neural circuitry. When using this integrative approach of data analysis, discrepancies, rather than being contradictory, provided a context to the cytoarchitecture of vLGN and dLGN.

Select PNN constituents are enriched in the developing vLGN

What emerged from proteomic analysis (and re-examination of transcriptomic analysis) was the discovery of an enrichment of ECM proteins, particularly CSPGs and glycoproteins associated with PNNs, in vLGN (Fig. 3a). This was unexpected, since immunostaining previously showed elevated expression of related ECM molecules, such as Aggrecan (ACAN), in the neonatal mouse dLGN (Brooks *et al.* 2013) (Figure S1). Here, we found a dramatic and significant increase in the number of mRNA transcripts for *Acan* across vLGN development (Fig. 3b), and these expression levels were significantly higher than in dLGN at the same timepoints (Fig. 3b). To confirm these results, we validated ACAN enrichment at the protein level by both Western Blot (with an antibody that detects the core of ACAN protein; AB1031) and immunohistochemistry (Figs 3c and 4).

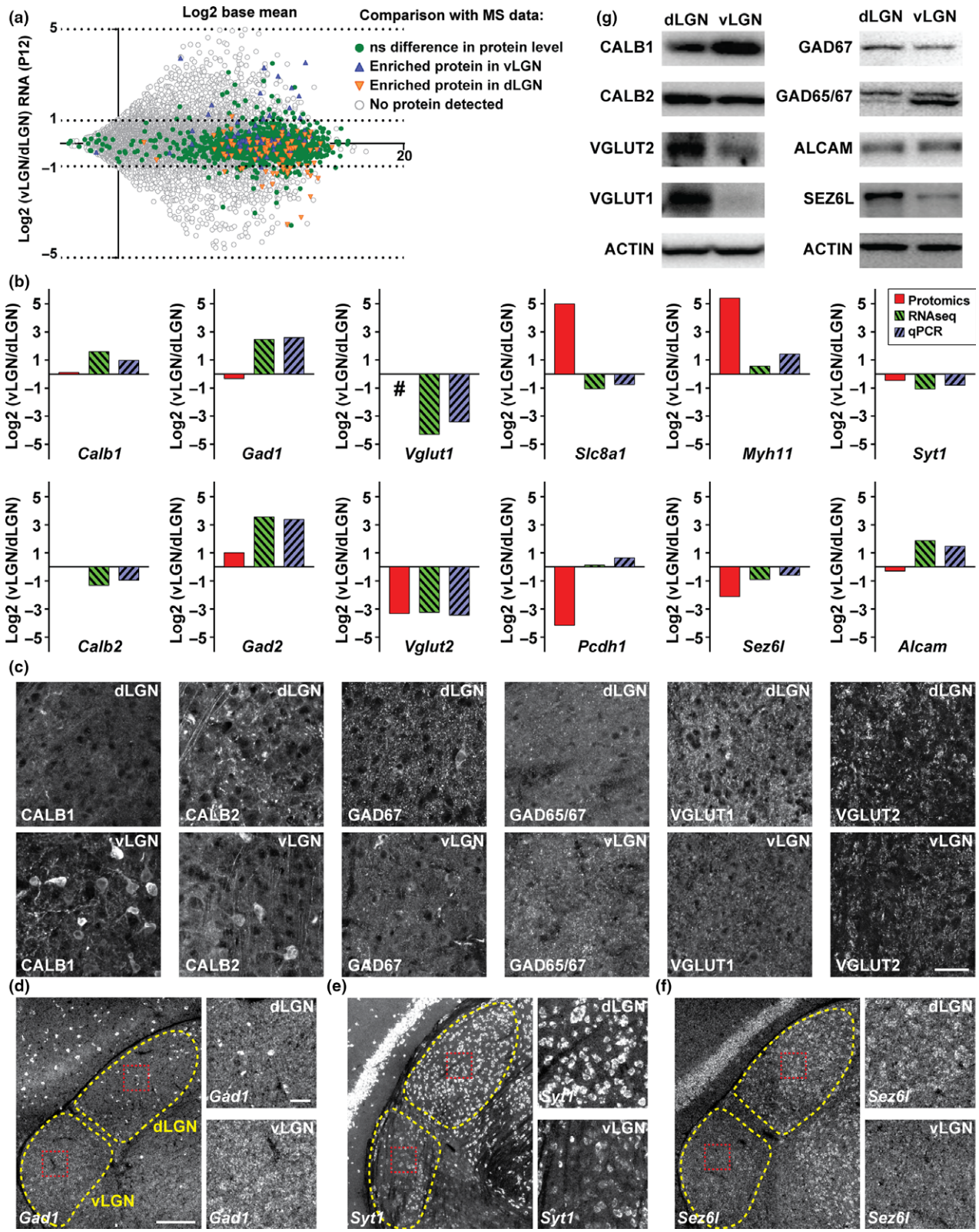

Acan was not the only PNN component that increased during vLGN development or was enriched in vLGN compared to dLGN at eye-opening. Protein levels of other CSPGs (e.g. Neurocan [NCAN], Phosphacan [PTPRZ1], versican [VCAN]), and Tenascin-C (TNC) were also enriched in vLGN (Fig. 3a). Previous immunohistochemical

Fig. 2 Comparison of differential proteomic and transcriptomic analysis of visual thalamus. (a) Volcano scatter plot mapping RNAseq expression differences between vLGN and dLGN at P12 obtained from RNAseq (Monavarfeshani *et al.* 2018) to proteomic data. Each data point is one mRNA transcript. Green circles indicate no significant differences in protein expression level associated with that mRNA, blue triangles indicate proteins enriched in vLGN, orange triangles indicate proteins enriched in dLGN, and blank circles indicate transcripts captured in RNAseq but not in mass-spectrometry (MS) datasets. (b) Comparison of expression data for select molecules obtained with quantitative PCR, RNAseq, and proteomics. # indicates no peptides detected by MS. (c) Immunohistochemical validation of expression of select proteins in (b). (d–f) *In situ* hybridization validating mRNA expression of select genes and peptides in (b). (g) WB analysis validating protein expression of select genes and peptides in (b). Calb1 – Calbindin 1; Calb2 – Calbindin 2; Gad1 – Glutamic acid decarboxylase; Gad2 – Glutamic acid decarboxylase 2; Vglut1 – Vesicular glutamate transporter 1; Vglut2 – Vesicular glutamate transporter 2; Slc8a1 – Sodium/calcium exchanger 1; Pcdh1 – Protocadherin 1; Myh11 – Myosin heavy chain 11; Sez6l – Seizure related 6 homolog like; Syt1 – Synaptotagmin 1; Alcam – Activated leukocyte cell adhesion molecule; GAD67 – Glutamic acid decarboxylase 67. Scale bars: (c) 40 μm, (d–f) 200 μm (inset 40 μm). All expression studies were performed at P12, $n = 3$ mice.

experiments supported these results as Phosphacan was enriched in vLGN compared to dLGN in neonatal mouse thalamus (Brooks *et al.* 2013). All of these ECM components (or their related family members) are associated with PNNs (Bandtlow and Zimmermann 2000; Yamaguchi 2000). In our transcriptome analysis, we found other key components of PNNs that were upregulated at eye-opening in vLGN and enriched in vLGN compared to dLGN (Fig. 3b, d–k). It is noteworthy that, while PNN components were enriched in vLGN, mRNAs of proteases known to degrade PNNs were enriched in dLGN (Levy *et al.* 2015). Specifically, A Disintegrin and Metalloproteinase with Thrombospondin motifs molecules (ADAMTS 1, 8, and 15) were enriched and upregulated in dLGN, potentially contributing to the scarceness of PNN proteins in this region (Fig. 3l–o).

WFA$^+$ and Cat315$^+$ PNNs exhibit different spatial and temporal expression patterns in vLGN

These results led us to hypothesize that there may be differences in PNN distribution in mouse vLGN and dLGN. To test this hypothesis, we investigated PNNs by immunolabelling with two antibodies directed against ACAN (AB1031 and Cat315, which labels a glycoform of ACAN [Matthews *et al.* 2002]) and by labeling PNNs with *Wisteria floribunda* agglutinin (WFA), an N-acetylgalactosamine-specific lectin (Härtig *et al.* 1992, 1994). We labeled PNNs with these approaches while also labeling retinal terminals in vLGN and dLGN by intraocular injection of fluorescent-conjugated Cholera Toxin subunit B (CTB). We identified two molecularly distinct populations of PNNs in visual thalamus: WFA$^+$Cat315$^-$ PNNs were present in the internal non-retinorecipient region of vLGN (vLGNi, Fig. 4e), and Cat315$^+$WFA$^-$ PNNs were present in the retinorecipient external region of vLGN (vLGNe; Fig. 4f). Importantly, both populations of PNNs in vLGN were labeled with AB1031, indicating they all contained ACAN, although the specific glycoforms of ACAN differed in these populations of PNNs. The molecular diversity of PNNs in vLGN was notable, since we found PNNs in most other cortical and subcortical brain regions were immunoreactive to both WFA and Cat315 antibodies (Fig. 4h–l′). We also found that the development of these distinct PNN populations differs, with WFA$^+$ PNNs emerging earlier than Cat315$^+$ PNNs (Figure S1). This result was not entirely surprising, given previous reports of the emergence of Cat315- and WFA-immunoreactivity in other brain regions (Ueno *et al.* 2017). A final observation was that immunolabeling with AB1031, Cat315, and WFA failed to identify PNNs in the mouse dLGN (Fig. S4a–d).

Although PNNs have been reported in the cat visual thalamus, they appear absent from the human LGN, despite the presence of ACAN (Sur *et al.* 1988; Hockfield *et al.* 1990; Lendvai *et al.* 2012). Instead, in human LGN, ACAN is enriched in perisynaptic axonal coats (Lendvai *et al.* 2012). We therefore explored whether the same was true in mouse visual thalamus. In contrast to human LGN, we found little evidence of Cat315 or WFA immunoreactivity in adult mouse dLGN, even outside of PNN-like structures (Figure S2). Previously, we reported diffuse ACAN was present in neonatal dLGN as retinal axons first invade visual thalamus, but this expression was lost during postnatal development as corticogeniculate axons invaded this thalamic region (Brooks *et al.* 2013; Seabrook *et al.* 2013) (see also Figure S1). Thus, since ACAN is lost in dLGN as retinogeniculate synapses form (Brooks *et al.* 2013) and prior to the formation of other non-retinal synapses (Bickford *et al.* 2010; Singh *et al.* 2012; Seabrook *et al.* 2013), it seems unlikely that ACAN participates in perisynaptic axonal coats in the neonatal mouse dLGN.

WFA$^+$ and Cat315$^+$ PNNs ensheath distinct neuronal types in vLGN

In many brain regions, PNNs primarily form around inhibitory Parvalbumin-expressing (PARV$^+$) interneurons (Wen *et al.* 2018). We tested whether WFA- or Cat315-immunoreactive PNNs ensheathed PARV$^+$ interneurons in vLGN. We labeled PARV$^+$ interneurons with either genetic labeling (in *Parv-Cre::Thy1-Stop-Yfp* mice) or immunostaining with anti-PARV antibodies (Fig. 5 and Figure S3). Both approaches revealed a small, regionally-restricted population of PARV$^+$ neurons in vLGNe (Fig. 5a and b and Figure S3).

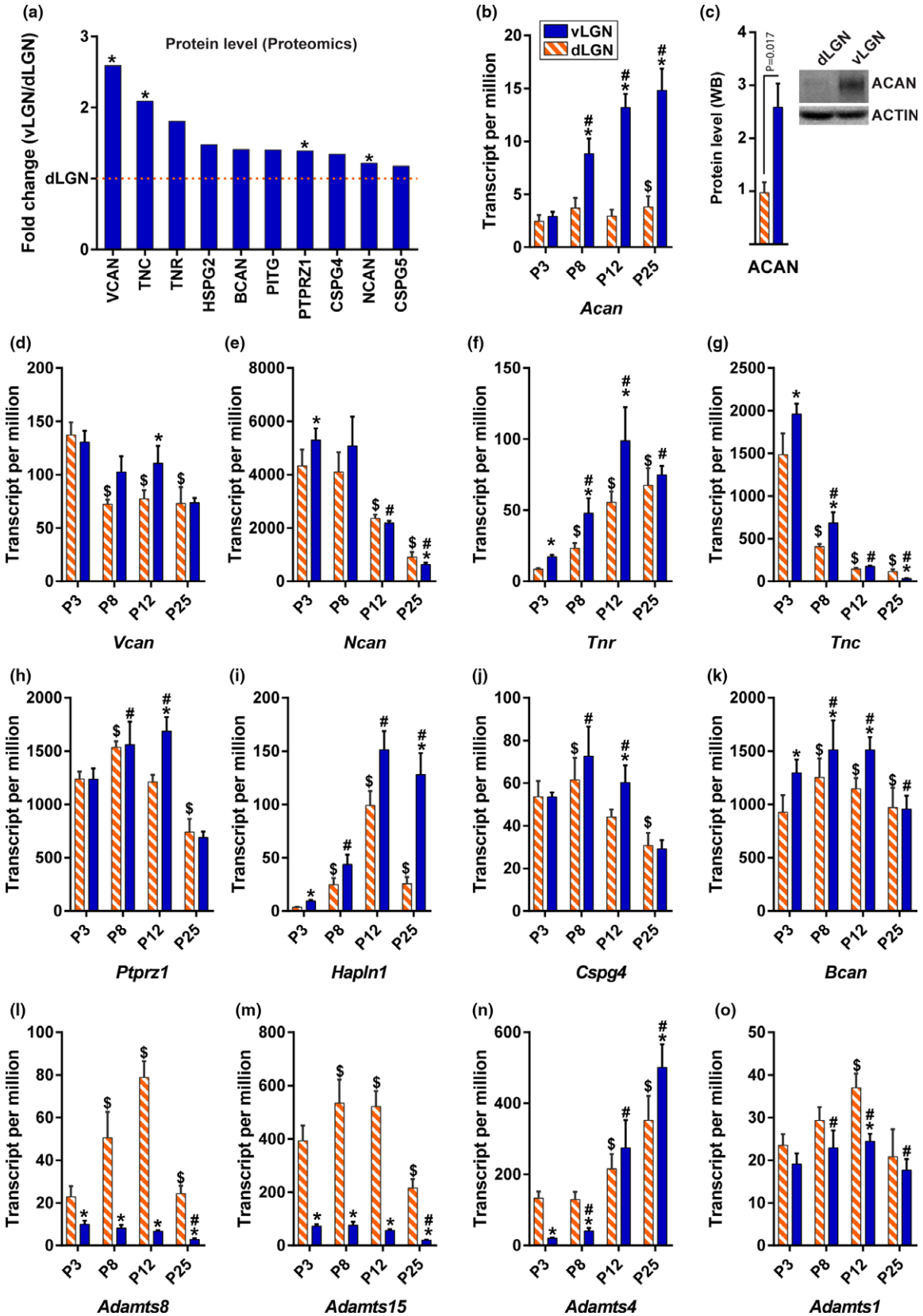
(a)
Protein level (Proteomics)
Fold change (vLGN/dLGN)
dLGN
VCAN
TNC
TNR
HSPG2
BCAN
PITG
PTPRZ1
CSPG4
NCAN
CSPG5
(b)
vLGN
dLGN
Transcript per million
P3
P8
P12
P25
Acan
(c)
P=0.017
dLGN
vLGN
ACAN
ACTIN
Protein level (WB)
ACAN
(d)
Vcan
(e)
Ncan
(f)
Tnr
(g)
Tnc
(h)
Ptprz1
(i)
Hapln1
(j)
Cspg4
(k)
Bcan
(l)
Adamts8
(m)
Adamts15
(n)
Adamts4
(o)
Adamts1

Fig. 3 Regulation of PNN component expression in the developing visual thalamus. (a) Differential protein expression in vLGN and dLGN at P12 captured by proteomic analysis. * indicates $p < 0.05$ when comparing expression levels in vLGN to dLGN (Student's *t*-test). (b) mRNA transcripts of *Acan* during development obtained from RNAseq. Data represent mean ± SEM. (c) Western Blot analysis and quantification of ACAN in adult mouse vLGN and dLGN. Data represent mean ± SEM. (d–o) mRNA transcripts of PNN components and proteases. Data represent mean ± SEM. * indicates $p < 0.05$ when comparing expression between vLGN and dLGN at this age. # and $ indicate $p < 0.05$ when comparing expression level in vLGN (#) or dLGN ($) with levels at P3 in the same region (Student's *t*-test). $n = 4$ mice. Acan – aggrecan; Bcan – brevican; Vcan – versican; Ncan – neurocan; Tnr – tenascin-r; Tnc – tenascin-c; Ptprz1 – phosphacan; Hapln1 – hyaluronan and proteoglycan binding link protein 1; Cspg4 – chondroitin sulfate proteoglycan 4; Hspg2 – heparan sulfate proteoglycan 2; Pitg – phosphatidylinositol glycan class A; Adamts8 – A disintegrin and metalloproteinase with thrombospondin motifs 8; Adamts15 – A disintegrin and metalloproteinase with thrombospondin motifs 15; Adamts4 – A disintegrin and metalloproteinase with thrombospondin motifs 4; Adamts1 – A disintegrin and metalloproteinase with thrombospondin motifs 1.

Few PARV$^+$ neurons were observed in dLGN, but PARV$^+$ axonal fibers were observed in this region (Fig. 5c).

Labeling in *Parv-Cre::Thy1-Stop-Yfp* mice revealed that WFA$^+$ PNNs surround the somata and proximal neurites of PARV$^+$ neurons in hippocampus, TRN, and visual cortex, as previously reported (Härtig *et al.* 1994; Su *et al.* 2017; Wen *et al.* 2018) (Fig. 5d–g). In contrast, PARV$^+$ interneurons in vLGN were not ensheathed by WFA$^+$ PNNs (Fig. 5a and b). We quantified these results and found that, while > 80% of YFP-expressing PARV$^+$ neurons were ensheathed by WFA$^+$ PNNs, < 10% of WFA$^+$ PNNs surround PARV$^+$ cells in vLGN (Fig. 5h). These results were replicated by IHC (Figure S3).

So what type of cells were ensheathed by WFA$^+$ PNNs in vLGN? We first ruled out the possibility that WFA$^+$ PNNs ensheath glial cells by visualizing astrocytes using an *Aldh1l1-GFP* reporter and microglia using an antibody against IBA1. As expected, neither cell type was surrounded by WFA$^+$ PNNs (Fig. 6a and b). Next, we tested whether other interneuron-types were ensheathed by WFA$^+$ PNNs. Specifically, we used immunolabeling and several genetic reporter lines to test colocalization with Neuropeptide Y (NPY$^+$), Somatostatin (Sst$^+$), Calbindin 1 (CALB1$^+$), Calbindin 2 (CALB2$^+$), and GAD67$^+$ interneurons. None of these interneurons appeared ensheathed by WFA$^+$ PNNs (Fig. 6c–j). Finally, we asked a more global question of whether WFA$^+$ PNNs in vLGN surround neurons at all. Neurons were labeled with antibodies against NeuN, and indeed we found that WFA$^+$ PNNs ensheath neurons in vLGN (Fig. 6k–l). At present, the specific type of neuron wrapped by WFA$^+$ PNNs in vLGN remains unknown.

We next turned our attention to investigate what cell-types are coated by Cat315$^+$ PNNs. Once again, we used a *Parv-Cre::Thy1-Stop-Yfp* transgenic reporter line and assessed the distribution of Cat315$^+$ PNNs (as well as WFA$^+$ PNNs). We found both WFA$^+$ and Cat315$^+$ ensheathed the same YFP$^+$ PARV$^+$ neurons in hippocampus, visual cortex, and TRN (Fig. 7a–c). Although WFA$^+$ PNNs were not (or rarely) observed around PARV$^+$ neurons, we discovered that PARV$^+$ interneurons in vLGN are ensheathed by Cat315$^+$ PNNs (Fig. 7e–f).

Cat315$^+$ PNN expression in vLGNe is reduced in the absence of retinogeniculate projections

A number of studies have shown that PNNs associated with regions of brain that process visual information, such as in cat visual thalamus and rodent visual cortex, form in an activity and experience-dependent manner (Sur *et al.* 1988; Kind *et al.* 1995; Ye and Miao 2013; Ueno *et al.* 2018). This led us to test whether the same applies to PNNs in mouse vLGN. We sought to determine whether PNN expression in visual thalamus was impacted by the loss of retinal input. It is worth noting here that the retinal projections to vLGN arrive neonatally and precede the formation of PNNs (Jaubert-Miazza *et al.* 2005; Fox and Guido 2011). To remove retinal inputs from vLGN (and all other retinorecipient regions) we utilized a targeted mouse mutant (*Math5*$^{-/-}$) in which RGCs fail to form (Wang *et al.* 2001). We assessed the distribution of PNNs in *Math5*$^{-/-}$ vLGN and found no significant change in the number or intensity of WFA$^+$ PNNs (Fig. 8a–c) or in other non-visual regions (Fig. S4). In contrast, we observed a significant reduction in Cat315$^+$ PNNs in *Math5*$^{-/-}$ vLGN in the absence of retinal inputs (Fig. 8d–f). Thus, a subset of PNNs within visual thalamus requires the presence of retinal inputs (and perhaps visual experience) for their timely formation.

Discussion

Here, we employed an integrative approach for analyzing unbiased proteomic and transcriptomic expression data from visual thalamus at eye-opening. These studies led us to investigate the composition, distribution, and development of PNNs in the LGN. While PNNs were absent from mouse dLGN, we discovered the presence of at least two molecularly-distinct PNNs in vLGN, each exhibiting different spatial and temporal expression patterns, and ensheathing non-overlapping subsets of neurons. Moreover, we found that the assembly of one of these classes of PNNs required the presence of retinal projections, suggesting their formation was activity-dependent.

It is worth noting that we were not able to identify many synaptogenic cues (at least previously well-characterized synaptogenic cues) in the developing visual thalamus

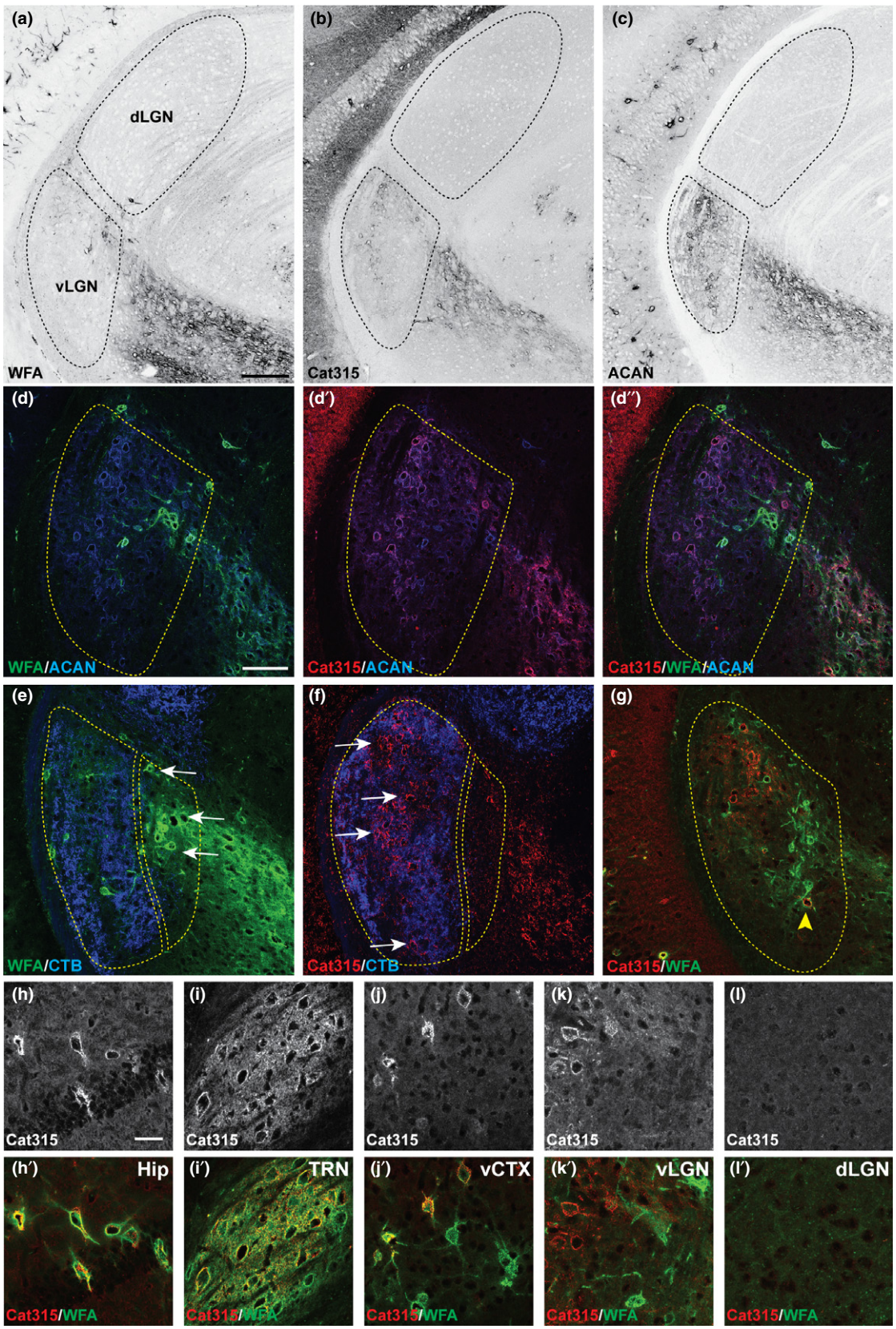
(a)
dLGN
vLGN
WFA
(b)
Cat315
(c)
ACAN
(d)
WFA/ACAN
(d′)
Cat315/ACAN
(d″)
Cat315/WFA/ACAN
(e)
WFA/CTB
(f)
Cat315/CTB
(g)
Cat315/WFA
(h)
Cat315
(i)
Cat315
(j)
Cat315
(k)
Cat315
(l)
Cat315
(h′)
Hip
Cat315/WFA
(i′)
TRN
Cat315/WFA
(j′)
vCTX
Cat315/WFA
(k′)
vLGN
Cat315/WFA
(l′)
dLGN
Cat315/WFA

Fig. 4 Distinct types and spatial distribution of PNNs in vLGN. (a) WFA-immunoreactivity, (b) Cat315-immunoreactivity, and (c) ACAN (AB1031)-immunoreactivity in adult mouse visual thalamus. (d–d'') Immunohistochemical validation of ACAN immunoreactivity in WFA^+ and $Cat315^+$ PNNs in vLGN. (e) Immunohistochemistry of WFA^+ PNNs and CTB-labeling of retinal terminals in P60 vLGN. (f) Immunohistochemistry of $Cat315^+$ PNNs and CTB-labeling of retinal terminals in P60 vLGN. (g) Immunohistochemistry of $Cat315^+$ and WFA^+ PNNs in vLGN. Few PNNs in vLGN co-label for WFA- and Cat315-immunoreactivity (rare example highlighted with yellow arrowhead). (h–l') High magnification images of immunostained $Cat315^+$ and WFA^+ PNNs in hip, thalamic reticular nucleus (TRN), vCTX, vLGN, and dLGN. Age P120. CTB – cholera toxin subunit B; WFA – *wisteria floribunda agglutinin*; TRN – thalamic reticular nucleus, vCTX – visual cortex; Hip – hippocampus. Scale bars: (a) 200 μm, (b) 100 μm, (d–h') 40 μm.

through our proteomic analysis, despite evidence that mRNAs of some such cues are differentially expressed in vLGN and dLGN (Su *et al.* 2011; Singh *et al.* 2012; Monavarfeshani *et al.* 2018). While advances in proteomics have dramatically contributed to our understanding of the brain proteome, current methodologies still lack the ability to capture the full breadth of peptides present in a sample (Chandramouli *et al.* 2009). For example, while membrane-bound proteins comprise a remarkable portion of the whole proteome (Wallin and Heijne 1998; Fagerberg *et al.* 2010), their identification through proteomic analysis has been challenging due to their unique biochemical properties. Likewise, proteomic approaches fall short in capturing many of the low abundant proteins (Vercauteren *et al.* 2004; Garbis *et al.* 2005). Additionally, the sophistication of neural circuitry, with its intricate architecture and far-reaching fibers, adds another layer of complexity to account for when interrogating nucleus-specific transcriptome and proteome (Ramadan *et al.* 2017). However, despite these technical limitations, our proteomic analysis captured a sizeable fraction of ECM- and membrane-associated proteins (Fig. 1c).

Of the plethora of molecules identified in both of our datasets, we turned our attention to extracellular proteins enriched in vLGN (Fig. 3a). We took interest in these molecules as our group and others have previously implicated ECM molecules in neuronal circuit formation and plasticity. PNNs were initially found coating cortical interneurons and were thought to function as restrictors of synaptic plasticity in inhibitory interneurons (Dityatev *et al.* 2010). A more recent report shows that dense PNN expression around excitatory pyramidal neurons in hippocampus suppresses plasticity (Carstens *et al.* 2016). Interestingly, other groups have shown that the window of plasticity can be reopened by degrading PNNs using ChABC in visual cortex and hyaluronidase in auditory cortex

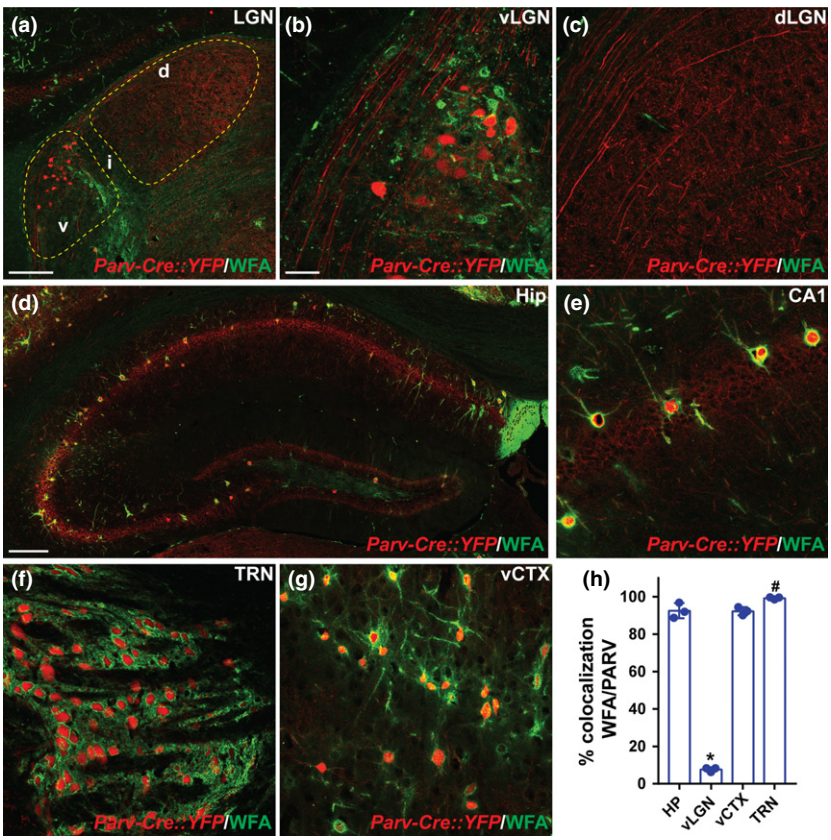

Fig. 5 $PARV^+$ vLGN neurons are not ensheathed by WFA^+ PNNs. (a) $PARV^+$ interneurons (red) in vLGN labeled in *Parv-Cre::Thy1-Stop-Yfp* mice are not ensheathed by WFA^+ PNNs (green). vLGN and dLGN are encircled by dashed lines. (b and c) High magnification images of WFA^+ PNNs and *Parv-Cre::Thy1-Stop-Yfp* labeled neurons in vLGN (b) and dLGN (c). (d–g) Immunostaining of WFA^+ PNNs surrounding $PARV^+$ interneurons in whole hippocampus (d), CA1 (e), thalamic reticular nucleus (TRN) (f), and visual cortex (g) of *Parv-Cre::Thy1-Stop-Yfp* mice. (h) Quantification of percent WFA^+ PNNs colocalizing with $PARV^+$ interneurons in different brain regions of *Parv-Cre::Thy1-Stop-Yfp* mice. Data represent mean ± SEM. $n = 3$ mice. * indicates $p < 0.0001$ when compared to all others, and # indicates $p < 0.05$ when compared to visual cortex and hippocampus (ANOVA). v – vLGN; i – IGL; d – dLGN; CA1 – Cornu Amonis 1; TRN – thalamic reticular nucleus. Scale bars: (a and d) 200 μm, (b,c, e–g) 40 μm.

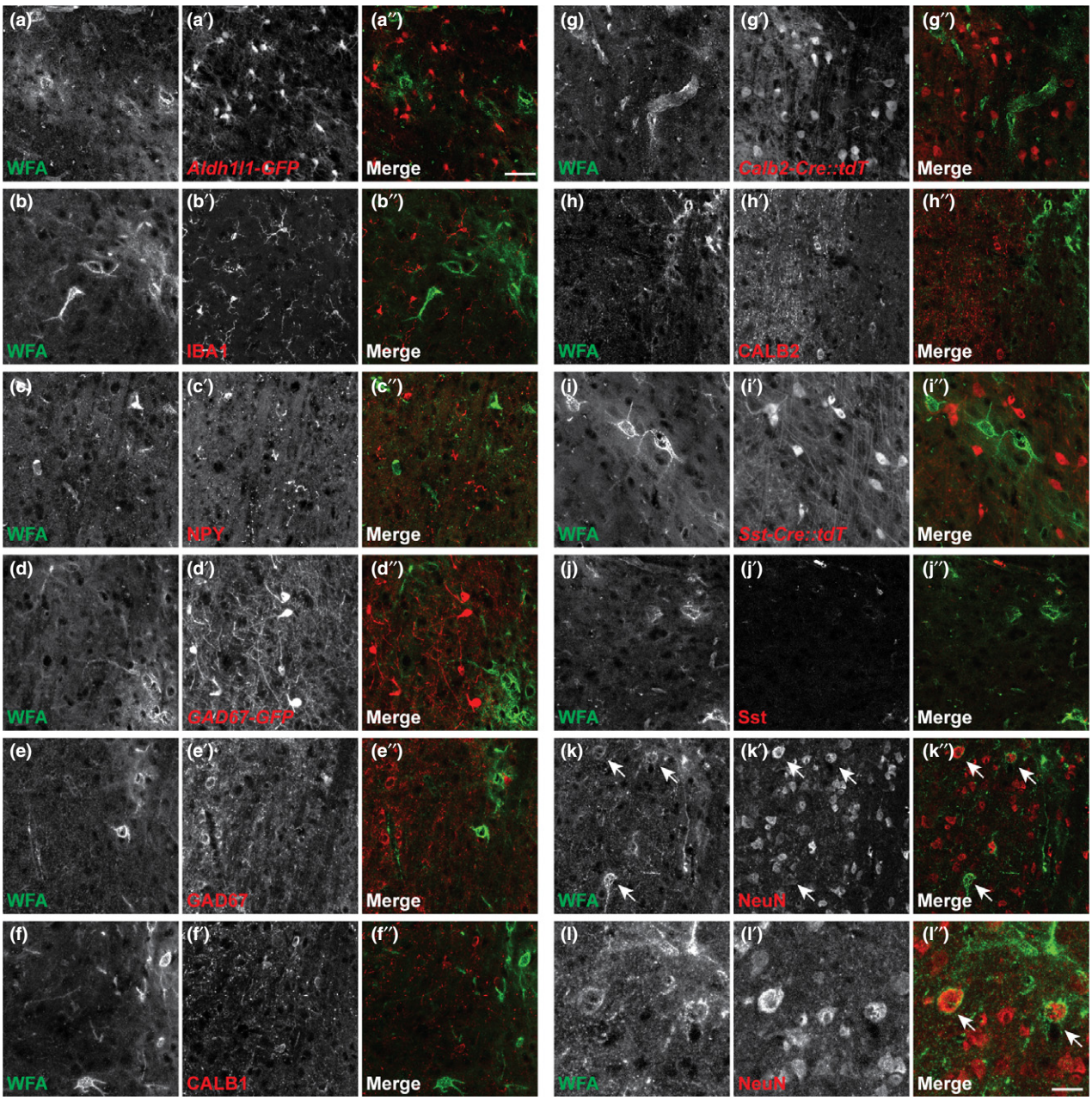

Fig. 6 WFA$^+$ PNNs ensheath neurons in vLGN. (a and b) Immunostaining of WFA$^+$ PNNs with labeled astrocytes in *Aldh1l1-GFP* mice (a) and immunostained IBA1$^+$ microglia (b). (c) Double immunostaining of WFA$^+$ PNNs with NPY$^+$ interneurons. (d–e) Immunostaining of WFA$^+$ PNNs with labeled GAD67$^+$ interneurons in *Gad67-GFP* mice (d) and immunolabeled GAD67$^+$ interneurons (e). (f) Double immunostaining of WFA$^+$ PNNs with CALB1$^+$ interneurons. (g–h) Immunostaining of WFA$^+$ PNNs with labeled calretinin-expressing interneurons in *Calb2-Cre::Rosa-Stop-Tdt* mice (g) and immunolabeled CALB2$^+$ interneurons (h). (i–j) Immunostaining of WFA$^+$ PNNs with labeled somatostatin-expressing interneurons in *Sst-Ires-Cre::Rosa-Stop-Tdt* mice (i) and Sst$^+$ interneurons (j). (k-l) Double immunostaining of WFA$^+$ PNNs with NeuN$^+$ neurons indicating colocalization at low magnification (K) and higher magnification (l). Aldh1l1 – Aldehyde dehydrogenase 1 family member l 1; IBA1 – Ionized calcium binding adaptor molecule 1; NPY – Neuropeptide Y; GAD67 – glutamic acid decarboxylase 67kD; CALB1 – Calbindin 1; Calb2 – Calbindin 2/Calretinin; Sst – Somatostatin; NeuN – Neuronal Nuclei. Scale bars: (a–k) 40 μm, (l) 20 μm.

(Pizzorusso *et al.* 2002; Happel *et al.* 2014). In terms of circuit formation, we previously reported a role for ACAN in regulating the timing of corticogeniculate innervation (Brooks *et al.* 2013). We have also demonstrated that ACAN-degrading metalloproteases (including ADAMTS 1, 4, 8, 15) exhibit distinct temporal and spatial expression patterns during early development, highlighting potential roles for ADAMTSs, a family of CSPG-degrading

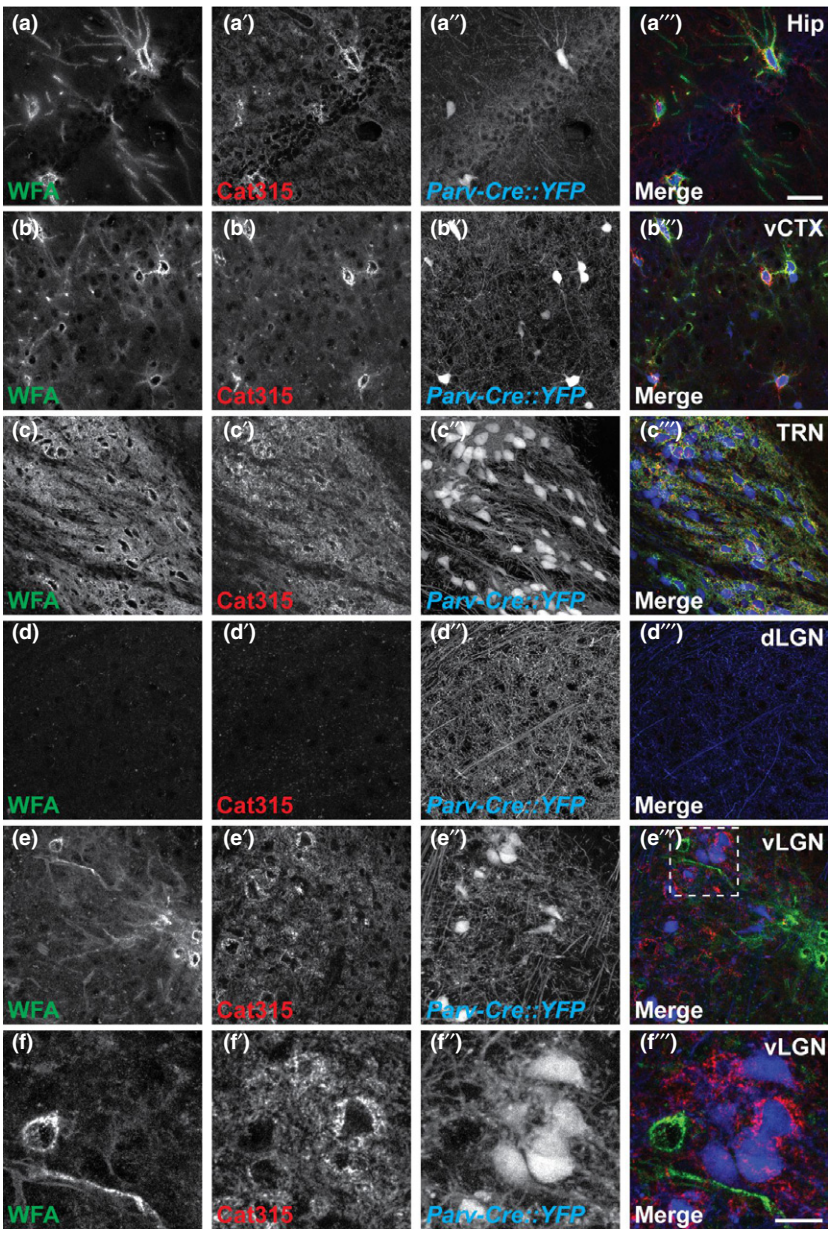

Fig. 7 Cat315$^+$ PNNs ensheath a subset of PARV$^+$ interneurons in vLGN. (a–d) Immunostained WFA$^+$ (green) and Cat315$^+$ (red) PNNs colocalize and ensheath PARV$^+$ interneurons in hippocampus (a), visual cortex (b), and thalamic reticular nucleus (TRN) (c) in *Parv-Cre::Thy1-Stop-Yfp* mice, with no WFA or Cat315 immunoreactivity detected in dLGN (d). (e) Immunostained Cat315$^+$ PNNs (red) ensheath PARV$^+$ interneurons in vLGN of in *Parv-Cre::Thy1-Stop-Yfp* mice. (f) Higher magnification of inset in (e). Scale bars: (a–e) 40 μm, (f) 20 μm.

metalloproteases, in visual thalamus development and function (Levy *et al.* 2015; Rossier *et al.* 2015). In fact, ADAMTS4, also known as Aggrecanase 1, is robustly generated in adult mouse visual thalamus by glial cells and by thalamic relay cells in the neonatal thalamus (Levy *et al.* 2015). Thus, although we have identified many molecules as being differentially expressed in vLGN and dLGN, we chose to focus on ECM proteins in our study, particularly on PNN components that were significantly enriched in our datasets.

A novel contribution of these studies is the identification of two types of PNNs which exhibit different spatial and temporal expression patterns in vLGN and which contain different glycoforms of ACAN. WFA$^+$ Cat315$^-$ PNNs are present in the non-retinorecipient vLGNi and WFA$^-$ Cat315$^+$ PNNs are present in the retinorecipient vLGNe. It should be noted that both WFA$^+$ Cat315$^-$ and WFA$^-$ Cat315$^+$ PNNs contain ACAN since they were both immunolabeled with AB1031 (Fig. 4). ACAN expression and modification is tightly regulated during development (Matthews *et al.* 2002; Dino *et al.* 2006) and is correlated with neural activity (Sur *et al.* 1988; Guimaraes *et al.* 1990; Kind *et al.* 1995; Lander *et al.* 1997; McRae *et al.* 2007, 2010). Why PNNs in vLGN contain different glycoforms of ACAN and what this might mean in terms of PNN or vLGN function, remains unknown.

Not only are their patterns of expression distinct, but Cat315$^+$ and WFA$^+$ PNNs also envelop different neuronal cell types in vLGN. While PARV$^+$ neurons are ensheathed

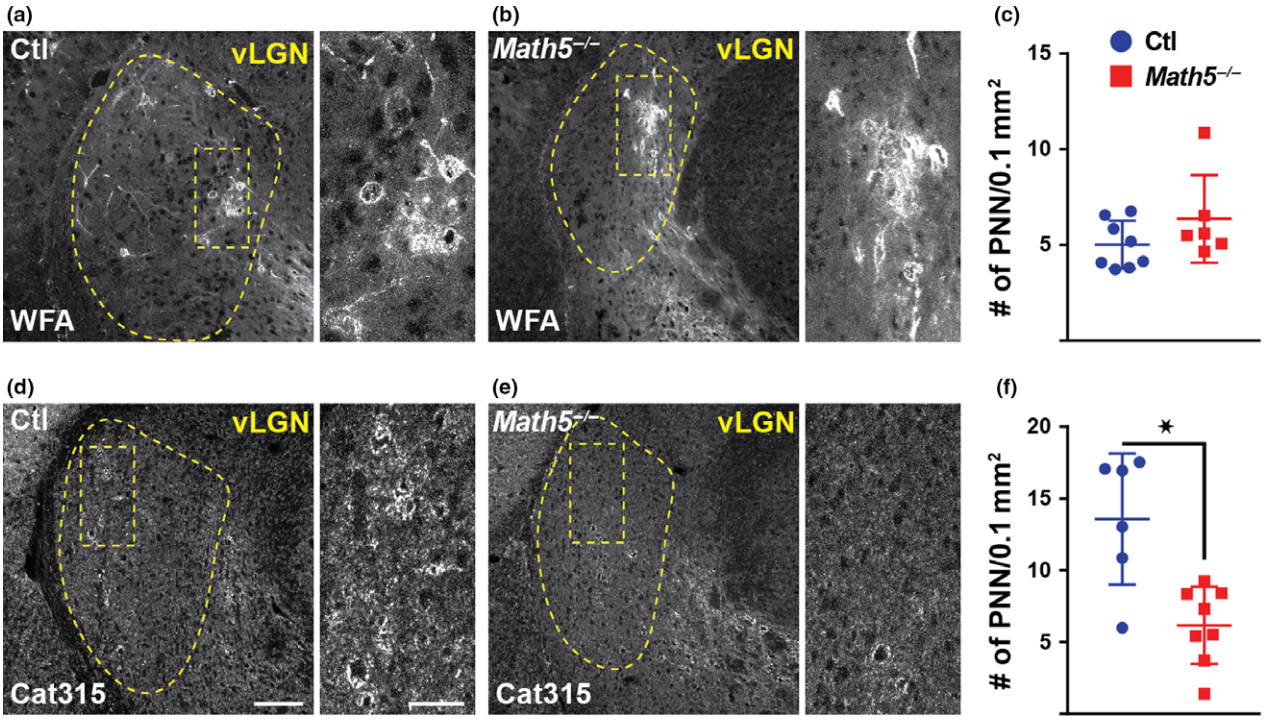

Fig. 8 Reduced Cat315$^+$ PNNs in vLGN in the absence of retinogeniculate projections. (a) WFA$^+$ PNN immunostaining in wildtype vLGN (left) with higher magnification of inset (right). (b) WFA$^+$ PNN immunostaining in vLGN of genetically blind (*Math5*$^{-/-}$) mutants (left) with higher magnification of inset (right). (c) Quantification of WFA$^+$ PNN density in wildtype and mutant vLGN. Data represent mean ± SD. * indicates $p < 0.05$ by (Student's *t*-test). (d) Cat315$^+$ PNNs in wildtype vLGN (left) with higher magnification of inset (right). (e) Cat315$^+$ PNNs in vLGN of genetically blind (*Math5*$^{-/-}$) mutants (left) with higher magnification of inset (right). (f) Quantification of Cat315$^+$ PNN density in wildtype and mutant vLGN. Data represent mean ± SD. $n \geq 6$ mice. Scale bar: (a and b, d–e) 100 μm (insets 40 μm).

by Cat315$^+$ PNNs, it remains unclear what specific neuronal types are coated by WFA$^+$Cat315$^-$ PNNs. While a large percentage of neurons in vLGN are GABAergic (Harrington 1997; Yuge *et al.* 2011), we found no overlap between GAD67-expressing cells and WFA$^+$ PNNs in vLGN. Thus, one possibility is that excitatory neurons (and not inhibitory interneurons) are ensheathed by PNNs in vLGNi. Unfortunately, the constellation of neuronal classes in the mouse vLGNi has not been well-documented.

Finally, we report here that Cat315$^+$ PNN expression in vLGNe is significantly reduced in *Math5*$^{-/-}$ mutants that lack retinal projections, while remaining unchanged in other regions of the *Math5*$^{-/-}$ mutant brain. This strongly suggests that the formation of this class of PNN in mouse visual thalamus is activity-dependent. Notably, other groups have also reported experience-dependent regulation of PNNs in select regions of brain. Ueno and colleagues showed an attenuation of WFA$^+$ PNNs surrounding PARV$^+$ interneurons in somatosensory cortex under sensory deprivation conditions (Ueno *et al.* 2017). Using immunostaining experiments in dark-reared mice, Ye and Miao reported a reduction of both WFA$^+$ and ACAN$^+$ PNNs in visual cortex (Ye and Miao 2013). Interestingly, we failed to detect changes in WFA$^+$ or Cat315$^+$ PNNs in visual cortex of *Math5*$^{-/-}$ mutants (Figure S5). This apparent discord could be due to several reasons. Dark-rearing, while an effective way of eliminating retinal activity, does not impose the same anatomical changes as genetic enucleation. In *Math5*$^{-/-}$ mice, retinal progenitors never differentiate into RGCs, preventing the formation of retinogeniculate synapses since early development, thus influencing downstream circuitry including thalamocortical projections and other efferents to visual cortex (Wang *et al.* 2001; Seabrook *et al.* 2013; El-Danaf *et al.* 2015). It is possible that the genetic removal of retinal inputs could lead to compensatory changes in visual circuits or function. Such changes may promote the normal development of PNNs in *Math5*$^{-/-}$ visual cortex. Finally, it warrants mention that, while we report the activity-dependent regulation of Cat315$^+$ PNNs, our results preclude us from drawing conclusions about whether WFA$^+$ PNN expression is regulated by activity since the driving inputs to the region of vLGN occupied by WFA$^+$ PNNs (i.e. vLGNi) are not retinal inputs. At present, driving inputs to vLGNi have yet to be defined, making it difficult to remove activity and assess PNN development in this region.

Taken together, the data we present shed new light on the ECM composition of mouse visual thalamus and raise new

questions about the role of PNNs in its development and function.

Acknowledgments and conflict of interest disclosure

This work was supported in part by the National Institutes of Health (EY021222 and EY024712 [MAF]), an Independent Investigator grant from the Brain and Behavior Foundation (MAF), and a fellowship from the VTCRI Medical Research Scholars Program (AM). All authors declare no actual or potential conflicts of interest.

All experiments were conducted in compliance with the ARRIVE guidelines.

Open science badges

This article has received a badge for *Open Materials* because it provided all relevant information to reproduce the study in the manuscript. The complete Open Science Disclosure form for this article can be found at the end of the article. More information about the Open Practices badges can be found at https://cos.io/our-services/open-science-badges/.

Supporting information

Additional supporting information may be found online in the Supporting Information section at the end of the article.

Figure S1. WFA+ PNNs precede the emergence of Cat315+ PNNs in vLGN.

Figure S2. Non-PNN associated Cat315- and WFA-immunoreactivity in adult mouse visual thalamus, hippocampus, and cerebral cortex.

Figure S3. PARV+ vLGN neurons are not ensheathed by WFA+ PNNs.

Figure S4. WFA+ PNNs ensheath select subsets of neurons in hippocampus.

Figure S5. Absence of retinal projections does not alter WFA+ and Cat315+ PNN expression in hippocampus and visual cortex.

References

Baden T., Berens P., Franke K., Rosón M. R., Bethge M. and Euler T. (2016) The functional diversity of retinal ganglion cells in the mouse. *Nature* **529**, 345–350.

Bandtlow C. E. and Zimmermann D. R. (2000) Proteoglycans in the developing brain: new conceptual insights for old proteins. *Physiol. Rev.* **80**, 1267–1290.

Bickford M. E., Slusarczyk A., Dilger E. K., Krahe T. E., Kucuk C. and Guido W. (2010) Synaptic development of the mouse dorsal lateral geniculate nucleus. *J. Comp. Neurol.* **518**, 622–635.

Bjartmar L., Huberman A. D., Ullian E. M. *et al.* (2006) Neuronal pentraxins mediate synaptic refinement in the developing visual system. *J. Neurosci.* **26**, 6269–6281.

Brooks J. M., Su J., Levy C., Wang J. S., Seabrook T. A., Guido W. and Fox M. A. (2013) A molecular mechanism regulating the timing of corticogeniculate innervation. *Cell Rep.* **5**, 573–581.

Brückner G., Brauer K., Härtig W. *et al.* (1993) Perineuronal nets provide a polyanionic, glia-associated form of microenvironment around certain neurons in many parts of the rat brain. *Glia* **8**, 183–200.

Carstens K. E., Phillips M. L., Pozzo-Miller L., Weinberg R. J. and Dudek S. M. (2016) Perineuronal nets suppress plasticity of excitatory synapses on CA2 pyramidal neurons. *J. Neurosci.* **36**, 6312–6320.

Celio M. R. and Blumcke I. (1994) Perineuronal nets—a specialized form of extracellular matrix in the adult nervous system. *Brain Res. Rev.* **19**, 128–145.

Celio M. R., Spreafico R., De Biasi S. and Vitellaro-Zuccarello L. (1998) Perineuronal nets: past and present. *Trends Neurosci.* **21**, 510–515.

Chandramouli K. and Qian P.-Y. (2009) Proteomics: challenges, techniques and possibilities to overcome biological sample complexity. Human genomics and proteomics: HGP, 2009.

Craig R. and Beavis R. C. (2004) TANDEM: matching proteins with tandem mass spectra. *Bioinformatics* **20**, 1466–1467.

Dino M., Harroch S., Hockfield S. and Matthews R. (2006) Monoclonal antibody Cat-315 detects a glycoform of receptor protein tyrosine phosphatase beta/phosphacan early in CNS development that localizes to extrasynaptic sites prior to synapse formation. *Neuroscience* **142**, 1055–1069.

Dityatev A. and Rusakov D. A. (2011) Molecular signals of plasticity at the tetrapartite synapse. *Curr. Opin. Neurobiol.* **21**, 353–359.

Dityatev A., Schachner M. and Sonderegger P. (2010) The dual role of the extracellular matrix in synaptic plasticity and homeostasis. *Nat. Rev. Neurosci.* **11**, 735.

El-Danaf R. N., Krahe T. E., Dilger E. K., Bickford M. E., Fox M. A. and Guido W. (2015) Developmental remodeling of relay cells in the dorsal lateral geniculate nucleus in the absence of retinal input. *Neural. Dev.* **10**, 19.

Fagerberg L., Jonasson K., von Heijne G., Uhlén M. and Berglund L. (2010) Prediction of the human membrane proteome. *Proteomics* **10**, 1141–1149.

Fox M. A. and Guido W. (2011) Shedding light on class-specific wiring: development of intrinsically photosensitive retinal ganglion cell circuitry. *Mol. Neurobiol.* **44**, 321–329.

Fox M. A. and Umemori H. (2006) Seeking long-term relationship: axon and target communicate to organize synaptic differentiation. *J. Neurochem.* **97**, 1215–1231.

Fox M. A., Sanes J. R., Borza D.-B. *et al.* (2007) Distinct target-derived signals organize formation, maturation, and maintenance of motor nerve terminals. *Cell* **129**, 179–193.

Frischknecht R., Heine M., Perrais D., Seidenbecher C. I., Choquet D. and Gundelfinger E. D. (2009) Brain extracellular matrix affects AMPA receptor lateral mobility and short-term synaptic plasticity. *Nat. Neurosci.* **12**, 897.

Frischknecht R. and Gundelfinger E. D. (2012) The brain's extracellular matrix and its role in synaptic plasticity, in *Synaptic Plasticity* In: (Kreutz M., Sala C. (eds)) pp. 153–171. Springer, Vienna.

Garbis S., Lubec G. and Fountoulakis M. (2005) Limitations of current proteomics technologies. *J. Chromatogr. A* **1077**, 1–18.

Guimaraes A., Zaremba S. and Hockfield S. (1990) Molecular and morphological changes in the cat lateral geniculate nucleus and visual cortex induced by visual deprivation are revealed by monoclonal antibodies Cat-304 and Cat-301. *J. Neurosci.* **10**, 3014–3024.

Hammer S., Carrillo G. L., Govindaiah G., Monavarfeshani A., Bircher J. S., Su J., Guido W. and Fox M. A. (2014) Nuclei-specific differences in nerve terminal distribution, morphology, and development in mouse visual thalamus. *Neural. Dev.* **9**, 16.

Hammer S., Monavarfeshani A., Lemon T., Su J. and Fox M. A. (2015) Multiple retinal axons converge onto relay cells in the adult mouse thalamus. *Cell Rep.* **12**, 1575–1583.

Happel M. F., Niekisch H., Rivera L. L. C., Ohl F. W., Deliano M. and Frischknecht R. (2014) Enhanced cognitive flexibility in reversal learning induced by removal of the extracellular matrix in auditory cortex. *Proc. Natl Acad. Sci.* **111**, 2800–2805.

Harrington M. E. (1997) The ventral lateral geniculate nucleus and the intergeniculate leaflet: interrelated structures in the visual and circadian systems. *Neurosci. Biobehav. Rev.* **21**, 705–727.

Härtig W., Brauer K. and Brückner G. (1992) Wisteria floribunda agglutinin-labelled nets surround parvalbumin-containing neurons. *NeuroReport* **3**, 869–872.

Härtig W., Brauer K., Bigl V. and Bru G. (1994) Chondroitin sulfate proteoglycan-immunoreactivity of lectin-labeled perineuronal nets around parvalbumin-containing neurons. *Brain Res.* **635**, 307–311.

Heikkinen A., Pihlajaniemi T., Faissner A. and Yuzaki M. (2014) Neural ECM and synaptogenesis, in *Progress in brain research* (Dityatev A., Wehrle-Haller B., Pitkänen A. eds), Vol. 214, pp. 29–51. Elsevier, Amsterdam.

Hockfield S., Kalb R., Zaremba S. and Fryer H. (1990) Expression of neural proteoglycans correlates with the acquisition of mature neuronal properties in the mammalian brain, in *Cold Spring Harbor Symposia on Quantitative Biology*, Vol. 55, pp. 505–514. Cold Spring Harbor Laboratory Press, New York.

Jaubert-Miazza L., Green E., Lo F.-S., Bui K., Mills J. and Guido W. (2005) Structural and functional composition of the developing retinogeniculate pathway in the mouse. *Vis. Neurosci.* **22**, 661–676.

Kind P., Beaver C. and Mitchell D. (1995) Effects of early periods of monocular deprivation and reverse lid suture on the development of cat-301 immunoreactivity in the dorsal lateral geniculate nucleus (dLGN) of the cat. *J. Comp. Neurol.* **359**, 523–536.

Krijgsveld J., Gauci S., Dormeyer W. and Heck A. J. (2006) In-gel isoelectric focusing of peptides as a tool for improved protein identification. *J. Proteome Res.* **5**, 1721–1730.

Kwok J. C., Carulli D. and Fawcett J. W. (2010) In vitro modeling of perineuronal nets: hyaluronan synthase and link protein are necessary for their formation and integrity. *J. Neurochem.* **114**, 1447–1459.

Land P. W., Kyonka E. and Shamalla-Hannah L. (2004) Vesicular glutamate transporters in the lateral geniculate nucleus: expression of VGLUT2 by retinal terminals. *Brain Res.* **996**, 251–254.

Lander C., Kind P., Maleski M. and Hockfield S. (1997) A family of activity-dependent neuronal cell-surface chondroitin sulfate proteoglycans in cat visual cortex. *J. Neurosci.* **17**, 1928–1939.

Lendvai D., Morawski M., Brückner G. *et al.* (2012) Perisynaptic aggrecan-based extracellular matrix coats in the human lateral geniculate body devoid of perineuronal nets. *J. Neurosci. Res.* **90**, 376–387.

Levy C., Brooks J., Chen J., Su J. and Fox M. (2015) Cell-specific and developmental expression of lectican-cleaving proteases in mouse hippocampus and neocortex. *J. Comp. Neurol.* **523**, 629–648.

Maier T., Güell M. and Serrano L. (2009) Correlation of mRNA and protein in complex biological samples. *FEBS Lett.* **583**, 3966–3973.

Martersteck E. M., Hirokawa K. E., Evarts M. *et al.* (2017) Diverse central projection patterns of retinal ganglion cells. *Cell Rep.* **18**, 2058–2072.

Matthews R. T., Kelly G. M., Zerillo C. A., Gray G., Tiemeyer M. and Hockfield S. (2002) Aggrecan glycoforms contribute to the molecular heterogeneity of perineuronal nets. *J. Neurosci.* **22**, 7536–7547.

McDonald J. H. (2009) *Handbook of Biological Statistics*. Sparky House Publishing Baltimore, MD.

McRae P. A., Rocco M. M., Kelly G., Brumberg J. C. and Matthews R. T. (2007) Sensory deprivation alters aggrecan and perineuronal net expression in the mouse barrel cortex. *J. Neurosci.* **27**, 5405–5413.

McRae P. A., Baranov E., Sarode S., Brooks-Kayal A. R. and Porter B. E. (2010) Aggrecan expression, a component of the inhibitory interneuron perineuronal net, is altered following an early-life seizure. *Neurobiol. Dis.* **39**, 439–448.

Monavarfeshani A., Knill C. N., Sabbagh U., Su J. and Fox M. A. (2017a) Region-and cell-specific expression of transmembrane collagens in mouse brain. *Front. Integr. Neurosci.* **11**, 20.

Monavarfeshani A., Sabbagh U. and Fox M. A. (2017b) Not a one-trick pony: diverse connectivity and functions of the rodent lateral geniculate complex. *Vis. Neurosci.* **34**, p. E012.

Monavarfeshani A., Stanton G., Su K., Mills III W. A., Swilling K., Kerr A., Huebschman N. A., Su J. and Fox M. A. (2018) LRRTM1 underlies synaptic convergence in visual thalamus. *eLife*, **7**, e33498.

Morawski M., Brückner G., Arendt T. and Matthews R. (2012) Aggrecan: beyond cartilage and into the brain. *Int. J. Biochem. Cell Biol.* **44**, 690–693.

Morgan J. L., Berger D. R., Wetzel A. W. and Lichtman J. W. (2016) The fuzzy logic of network connectivity in mouse visual thalamus. *Cell* **165**, 192–206.

Morin L. P. and Studholme K. M. (2014) Retinofugal projections in the mouse. *J. Comp. Neurol.* **522**, 3733–3753.

Neilson K. A., Keighley T., Pascovici D., Cooke B. and Haynes P. A. (2013) Label-free quantitative shotgun proteomics using normalized spectral abundance factors. in *Proteomics for Biomarker Discovery* (Zhou M., Veenstra T. eds), pp. 205–222. Humana Press, Totowa, NJ.

Osterhout J. A., Josten N., Yamada J. *et al.* (2011) Cadherin-6 mediates axon-target matching in a non-image-forming visual circuit. *Neuron* **71**, 632–639.

Pizzorusso T., Medini P., Berardi N., Chierzi S., Fawcett J. W. and Maffei L. (2002) Reactivation of ocular dominance plasticity in the adult visual cortex. *Science* **298**, 1248–1251.

Rabilloud T. (2003) Membrane proteins ride shotgun. Nature Publishing Group. *Nat. Biotechnol.* **21**, 508–510.

Ramadan N., Ghazale H., El-Sayyad M., El-Haress M. and Kobeissy F. H. (2017) Neuroproteomics studies: challenges and updates. *Neuroproteomics*, **1598**, 3–19.

Rheaume B. A., Jereen A., Bolisetty M., Sajid M. S., Yang Y., Renna K., Sun L., Robson P. and Trakhtenberg E. F. (2018) Single cell transcriptome profiling of retinal ganglion cells identifies cellular subtypes. *Nat. Commun.* **9**, 2759.

Risher W. C. and Eroglu C. (2012) Thrombospondins as key regulators of synaptogenesis in the central nervous system. *Matrix Biol.* **31**, 170–177.

Rossier J., Bernard A., Cabungcal J. *et al.* (2015) Cortical fast-spiking parvalbumin interneurons enwrapped in the perineuronal net express the metallopeptidases Adamts8, Adamts15 and Neprilysin. *Mol. Psychiatry* **20**, 154.

Sanes J. R. and Masland R. H. (2015) The types of retinal ganglion cells: current status and implications for neuronal classification. *Annu. Rev. Neurosci.* **38**, 221–246.

Sanes J. R. and Yamagata M. (2009) Many paths to synaptic specificity. *Annu. Rev. Cell Dev. Biol.* **25**, 161–195.

Schmittgen T. D. and Livak K. J. (2008) Analyzing real-time PCR data by the comparative CT method. *Nat. Protoc.* **3**, 1101–1108.

Seabrook T. A., El-Danaf R. N., Krahe T. E., Fox M. A. and Guido W. (2013) Retinal input regulates the timing of corticogeniculate innervation. *J. Neurosci.* **33**, 10085–10097.

Shevchenko A., Tomas H., Havli J., Olsen J. V. and Mann M. (2006) In-gel digestion for mass spectrometric characterization of proteins and proteomes. *Nat. Protoc.* **1**, 2856.

Shevchenko G., Musunuri S., Wetterhall M. and Bergquist J. (2012) Comparison of extraction methods for the comprehensive analysis of mouse brain proteome using shotgun-based mass spectrometry. *J. Proteome Res.* **11**, 2441–2451.

Singh R., Su J., Brooks J., Terauchi A., Umemori H. and Fox M. A. (2012) Fibroblast growth factor 22 contributes to the development of retinal nerve terminals in the dorsal lateral geniculate nucleus. *Frontiers in Molecular Neuroscience*, **4**, 61.

Smith P. D., Coulson-Thomas V. J., Foscarin S., Kwok J. C. and Fawcett J. W. (2015) "GAG-ing with the neuron": the role of glycosaminoglycan patterning in the central nervous system. *Exp. Neurol.* **274**, 100–114.

Sorg B. A., Berretta S., Blacktop J. M., Fawcett J. W., Kitagawa H., Kwok J. C. and Miquel M. (2016) Casting a wide net: role of perineuronal nets in neural plasticity. *J. Neurosci.* **36**, 11459–11468.

van't Spijker H. M. and Kwok J. C. (2017) A sweet talk: the molecular systems of perineuronal nets in controlling neuronal communication. *Front. Integr. Neurosci.* **11**, 33.

Stevens B., Allen N. J., Vazquez L. E. *et al.* (2007) The classical complement cascade mediates CNS synapse elimination. *Cell* **131**, 1164–1178.

Su J., Gorse K., Ramirez F. and Fox M. A. (2010) Collagen XIX is expressed by interneurons and contributes to the formation of hippocampal synapses. *J. Comp. Neurol.* **518**, 229–253.

Su J., Haner C. V., Imbery T. E., Brooks J. M., Morhardt D. R., Gorse K., Guido W. and Fox M. A. (2011) Reelin is required for class-specific retinogeniculate targeting. *J. Neurosci.* **31**, 575–586.

Su J., Cole J. and Fox M. A. (2017) Loss of interneuron-derived collagen XIX leads to a reduction in perineuronal nets in the mammalian telencephalon. *ASN Neuro* **9**.

Sur M., Garraghty P. E. and Roe A. W. (1988) Experimentally induced visual projections into auditory thalamus and cortex. *Science* **242**, 1437–1441.

Ueno H., Suemitsu S., Okamoto M., Matsumoto Y. and Ishihara T. (2017) Sensory experience-dependent formation of perineuronal nets and expression of Cat-315 immunoreactive components in the mouse somatosensory cortex. *Neuroscience* **355**, 161–174.

Ueno H., Fujii K., Suemitsu S. *et al.* (2018) Expression of aggrecan components in perineuronal nets in the mouse cerebral cortex. *IBRO Reports* **4**, 22–37.

Vercauteren F. G., Bergeron J. J., Vandesande F., Arckens L. and Quirion R. (2004) Proteomic approaches in brain research and neuropharmacology. *Eur. J. Pharmacol.* **500**, 385–398.

Waites C. L., Craig A. M. and Garner C. C. (2005) Mechanisms of vertebrate synaptogenesis. *Annu. Rev. Neurosci.* **28**, 251–274.

Wallin E. and Heijne G. V. (1998) Genome-wide analysis of integral membrane proteins from eubacterial, archaean, and eukaryotic organisms. *Protein Sci.* **7**, 1029–1038.

Wang S. W., Kim B. S., Ding K., Wang H., Sun D., Johnson R. L., Klein W. H. and Gan L. (2001) Requirement for math5 in the development of retinal ganglion cells. *Genes Dev.* **15**, 24–29.

Wen T. H., Binder D. K., Ethell I. M. and Razak K. A. (2018) The Perineuronal 'Safety'Net? Perineuronal Net Abnormalities in Neurological Disorders. *Frontiers in Molecular Neuroscience* **11**, 270.

Yamaguchi Y. (2000) Lecticans: organizers of the brain extracellular matrix. *Cell. Mol. Life Sci.* **57**, 276–289.

Ye Q. and Miao Q.-L. (2013) Experience-dependent development of perineuronal nets and chondroitin sulfate proteoglycan receptors in mouse visual cortex. *Matrix Biol.* **32**, 352–363.

Yogev S. and Shen K. (2014) Cellular and molecular mechanisms of synaptic specificity. *Annu. Rev. Cell Dev. Biol.* **30**, 417–437.

Yuge K., Kataoka A., Yoshida A. C., Itoh D., Aggarwal M., Mori S., Blackshaw S. and Shimogori T. (2011) Region-specific gene expression in early postnatal mouse thalamus. *J. Comp. Neurol.* **519**, 544–561.

Zimmermann D. R. and Dours-Zimmermann M. T. (2008) Extracellular matrix of the central nervous system: from neglect to challenge. *Histochem. Cell Biol.* **130**, 635–653.

Open Practices Disclosure

Manuscript Title: Distribution and development of molecularly distinct perineuronal nets in visual thalamus
Corresponding Author: Michael A. Fox

Articles accepted to *Journal of Neurochemistry* after 01.2018 are eligible to earn badges that recognize open scientific practices: publicly available data, material, or preregistered research plans. Please read more about the badges in our *author guidelines and Open Science Badges page*, and you can also find information on the Open Science Framework wiki.

[X] Please check this box if you are interested in participating.

To apply for one or more badges acknowledging open practices, please check the box(es) corresponding to the desired badge(s) below and provide the information requested in the relevant sections. To qualify for a badge, you must provide a URL, doi, or other permanent path for accessing the specified information in a public, open-access repository. **Qualifying public, open-access repositories are committed to preserving data, materials, and/or registered analysis plans and keeping them publicly accessible via the web in perpetuity.** Examples include the Open Science Framework (OSF) and the various Dataverse networks. Hundreds of other qualifying data/materials repositories are listed at http://re3data.org/. Preregistration of an analysis plan must take place via a publicly accessible registry system (e.g., OSF, ClinicalTrials.gov or other trial registries in the WHO Registry Network, institutional registration systems). **Personal websites and most departmental websites do not qualify as repositories.**

Authors who wish to publicly post third-party material in their data, materials, or preregistration plan must have the proper authority or permission agreement in order to do so.

There are circumstances in which it is not possible or advisable to share any or all data, materials, or a research plan publicly. For example, there are cases in which sharing participants' data could violate confidentiality. If you would like your article to include an explanation of such circumstances and/or provide links to any data or materials you have made available—even if not under conditions eligible to earn a badge—you may write an alternative note that will be published in a note in the article. Please check this box if you would like your article to include an alternative note and provide the text of the note below:

[] Alternative note:

[] Open Data Badge

1. Provide the URL, doi, or other **permanent path** for accessing the data in a **public, open-access repository**:

[] Confirm that there is sufficient information for an independent researcher to reproduce **all of the reported results**, including codebook if relevant.

[] Confirm that you have registered the uploaded files so that they are **time stamped** and cannot be age.

[X] Open Materials Badge

1. Provide the URL, doi, or other **permanent path** for accessing the materials in a **public, open-access repository**: all relevant information is provided in the manuscript.

[X] Confirm that there is sufficient information for an independent researcher to reproduce **all of the reported methodology**.

[] Confirm that you have registered the uploaded files so that they are **time stamped** and cannot be age.

[] Preregistered Badge

1. Provide the URL, doi, or other **permanent path** to the registration in a **public, open-access repository***:

2. Was the analysis plan registered prior to examination of the data or observing the outcomes? If no, explain.**

3. Were there additional registrations for the study other than the one reported? If yes, provide links and explain.*

*No badge will be awarded if (1) is not provided, **or** if (3) is answered "yes" without strong justification

**If the answer to (2) is "no," the notation DE (Data Exist) will be added to the badge, indicating that registration postdates realization of the outcomes but predates analysis.

By signing below, authors affirm that the above information is accurate and complete, that any third-party material has been reproduced or otherwise made available only with the permission of the original author or copyright holder, and that publicly posted data do not contain information that would allow individuals to be identified without consent.

Date: 10/10/18

Name: Michael A. Fox

Signature: